

~~CONFIDENTIAL~~

Copy  
RM L

1960  
SEP 19 1960

0144790



TECH LIBRARY KAPB, NM

NACA RM L57F27

68LL

~~CONFIDENTIAL~~  
**NACA**

# RESEARCH MEMORANDUM

TEMPERATURE MEASUREMENTS FROM A FLIGHT TEST OF TWO  
WING-BODY COMBINATIONS AT 7° ANGLE OF ATTACK FOR  
MACH NUMBERS TO 4.86 AND REYNOLDS  
NUMBERS TO  $19.2 \times 10^6$

By Leo T. Chauvin

Langley Aeronautical Laboratory  
Langley Field, Va.

~~CONFIDENTIAL~~  
CLASSIFIED DOCUMENT

~~THIS INFORMATION IS UNCLASSIFIED EXCEPT WHERE SHOWN OTHERWISE BY A DATE AND AUTHORITY. IT IS THE POLICY OF THE UNITED STATES GOVERNMENT TO MAKE ALL INFORMATION CONTAINED HEREIN AVAILABLE TO THE PUBLIC UNLESS IT IS DETERMINED THAT DISCLOSURE OF THE INFORMATION IS UNDESIRABLE IN THE INTERESTS OF NATIONAL DEFENSE. IN ANY EVENT, DISCLOSURE OF THIS INFORMATION TO AN UNAUTHORIZED PERSON IS PROHIBITED BY LAW.~~

**NATIONAL ADVISORY COMMITTEE  
FOR AERONAUTICS**

WASHINGTON

September 12, 1957

~~CONFIDENTIAL~~

~~CONFIDENTIAL~~



## NATIONAL ADVISORY COMMITTEE FOR AERONAUTICS

## RESEARCH MEMORANDUM

TEMPERATURE MEASUREMENTS FROM A FLIGHT TEST OF TWO  
WING-BODY COMBINATIONS AT 7° ANGLE OF ATTACK FOR  
MACH NUMBERS TO 4.86 AND REYNOLDS  
NUMBERS TO  $19.2 \times 10^6$

By Leo T. Chauvin

## SUMMARY

A temperature survey is presented for two bodies having wings swept 39° and 75° for an angle of attack of 7°, Mach numbers up to 4.86, and a free-stream Reynolds number per foot of  $19.2 \times 10^6$ . Effects of wing-body interference on the heating of the body are indicated as well as the difference in heating on windward and leeward sides at angle of attack. Pressure coefficients are also presented for the windward and leeward sides of the body for two stations on the body.

## INTRODUCTION

The designer of supersonic aircraft is confronted not only with the analysis of the heating of isolated airplane components but with these components in combination. For moderate Mach numbers, heat-transfer theory has been shown to be adequate for the prediction of the aerodynamic heating to simple bodies and wings; however, very little heat-transfer information (theory or experimental) exists on the effects of wing-body interference, particularly at angles of attack.

Some heat-transfer results from wind-tunnel tests for bodies at angles of attack of 7° and 25° have been presented in reference 1. In order to provide heat-transfer information at an angle of attack from flight tests, a new technique was developed whereby two test models were mounted at 7° angle of attack to the forward end of a rocket motor in a forklike arrangement in such a way that the lift on one model was nullified by the lift on the other model. This report presents the preliminary results of the first flight test of a system of this type.

The data presented are for a Mach number of 4.86 and a Reynolds number per foot of  $19.2 \times 10^6$ . Temperature time histories are presented along with other data necessary to reduce the temperature measurements to heat-transfer rates.

This flight test was conducted at the Langley Pilotless Aircraft Research Station at Wallops Island, Va., on April 10, 1957.

#### SYMBOLS

$C_p$	pressure coefficient, $\frac{p_l - p_\infty}{0.7 p_\infty M^2}$
$c$	wing chord
$M$	Mach number
$p$	pressure, lb/sq in.
$R$	Reynolds number per foot
$T$	temperature, $^{\circ}F$ or $^{\circ}R$
$\Lambda$	angle of sweep, deg
$\alpha$	angle of attack, deg
$\phi$	azimuthal location of temperature pickup measured from meridional plane, deg
$\rho$	density, slugs/cu ft
$t$	time, sec
$x$	horizontal distance from wing leading edge
Subscripts:	
$\infty$	free stream
$w$	pertaining to wall
$t,2$	total pressure behind normal shock
$l$	local

~~CONFIDENTIAL~~

## MODELS, INSTRUMENTATION, AND FLIGHT TESTS

The models are shown in launching position in figure 1(a). The propulsion system consisted of an M6 JATO Honest John booster rocket for the first stage and an M5 JATO Nike rocket for the second stage. The test models shown in figures 1(b) and 1(c) consisted of two ogival-nose cylinders; one model had  $39^\circ$  swept wings and the other had  $75^\circ$  swept wings. These models were mounted on the forward end of the Nike booster which was stabilized by four fins equally spaced about the rearward end of the rocket motor. In order to provide testing at an angle of attack of  $7^\circ$ , the models were fixed in a forklike arrangement as illustrated (fig. 1(a)). A sketch of the models is shown in figure 2 and nose coordinates and skin thicknesses are given in table I. In order to provide thin skin in the wing-body region, the forces due to lift on the wings were transmitted to an inner body made of phenolic-glass fiber. A groove  $1/2$  inch by  $1/4$  inch extending the length of the wing section was provided in the phenolic-glass inner body to minimize heat losses from the thermocouple stations located on the metal body shell. The wings were solid steel and in order to make heat-transfer measurements close to the wing root, the wing surface at the thermocouple stations was undercut to half the wing thickness and heat-transfer panels were then installed flush to the wing surface. Metal-to-metal contact was prevented by a Micarta insulator placed between the wing main structure and the heat panels. These cutouts in the wing are indicated in figure 2, and the heat panels are visible in the photographs of the models (figs. 1(b) and (c)).

## Instrumentation

An NACA 10-channel telemeter was carried in the model adapter section and transmitted wall temperatures, pressures, and normal and transverse acceleration to ground receiving stations. The 51 temperature pickups were commutated at approximately 0.25 second. Number 30 chromel-alumel thermocouples were welded to the inner surface of the skin at the stations given in table II. Thermocouple locations are also shown in figures 2(a) and (b). Five of the channels transmitted continuous readings of absolute pressure. The measurement at station A was total pressure, whereas at stations B and C, measurements were made at 5 and 10 inches from the stagnation point, respectively, and at  $180^\circ$  from each other. The remaining two channels transmitted continuous readings of normal and transverse acceleration.

Trajectory data were obtained by using an NACA modified SCR-584 position radar. Atmospheric and wind conditions were measured by means of radiosondes launched near the time of flight and tracked by a Rawin set AN/GMD-1A. Model velocity was obtained from CW Doppler radar,

pitot-tube relation, and from the position radar. Atmospheric conditions as obtained from radiosonde measurements are presented in figure 3 along with the altitude time history of the model for 30 seconds of flight.

#### Flight Tests

The models were propelled by a two-stage system (Honest John-Nike) as described in the section entitled "Models." At burnout of the first stage the test vehicle had reached a Mach number of 2.1, and following a short coast period the ignition of the Nike motor accelerated the models to a Mach number of 4.86. The normal and transverse accelerometers indicated that the configuration flew at zero lift trajectory except at close to peak Mach number where the model yawed in the plane normal to that of the wedge adapter to which the models were attached. This yawing resulted in an angle of attack which was estimated to be less than  $1^\circ$ . The variation of Mach number and free-stream Reynolds number per foot is presented as a function of time in figure 4. The configuration was launched at an angle of  $75^\circ$ .

#### RESULTS AND DISCUSSION

The variation of measured wall temperature with time is presented in figures 5 and 6. Temperature time histories are presented in figure 5 for the wing and wing-body region of the model with  $75^\circ$  swept wings. In figure 6, temperature time histories are presented for stations on the wing, the body forward of the wing, and the wing-body region for the model with  $39^\circ$  swept wings.

Figure 7 shows the temperature distribution along the body of the model with  $39^\circ$  of wing sweep for a peak Mach number of 4.86 corresponding to a flight time of 10.2 seconds. The distribution along the windward side  $\phi = 0^\circ$  shows a rapid decrease in temperature up to 10 inches from the nose (which is the measurement station just ahead of the fins). At the next station, which is located in the wing-body region, the wall-temperature trend from the previous stations is reversed and increases approximately  $100^\circ$  F over the entire region. A similar trend for the leeward side of the body is shown. Preliminary results of the heat-transfer tests for stations at 5 and 10 inches from the nose have indicated turbulent flow, thereby showing that the reversal in the temperature curve is not attributed to boundary-layer transition but to wing-body interference. Shown in the figure are temperature distributions made on the body for  $\phi = 67.5^\circ$  and  $112.5^\circ$  which are  $22\frac{1}{2}^\circ$  from the wing root for the windward and leeward sides, respectively. The windward side

$\phi = 67.5^\circ$  shows an increase of  $255^\circ$  F from 15.3 to 23.5 inches which may suggest a wing-body effect. A similar effect was also indicated for the wing-body model with  $\Lambda = 75^\circ$ . The leeward side of the body at  $\phi = 122.5^\circ$  shows no appreciable differences from the distribution for  $\phi = 180^\circ$ .

The distribution of skin temperature around the body is shown in the figure for stations at 5 and 10 inches from the nose. The points are indicated by the thermocouple number which is further identified by the sketch at the top of the figure. For the stations at 5 inches from nose, the temperature is highest at the windward point  $\phi = 0^\circ$  and decreases gradually around the surface to  $\phi = 180^\circ$  (leeward). For stations at 10 inches from the nose, the distribution is different in that the highest temperature occurs  $45^\circ$  from the windward side. This is illustrated better in figure 8 where the temperature around the body at each station is plotted as a function of angular distance. This significant change in the distribution of temperature may be explained when the crossflow heat-transfer coefficients are evaluated.

Figure 9 presents the temperature distribution for the  $39^\circ$  and  $75^\circ$  swept wings at an angle of attack of  $7^\circ$ . The effect of angle of attack of the wing on the heat transfer is evident by the large differences in skin temperature between the windward and leeward sides of the wing. Shown also are the leading-edge temperatures measured at 0.8 inch from the body for the  $75^\circ$  swept wing and at 0.9 inch from the body for the  $39^\circ$  swept wing.

Figure 10 presents the time histories of the wing leading-edge temperature for the two wings and for the body nose tip. The lower temperature of the body nose tip is due to the thicker skin at this station.

Pressure coefficients for stations at 5 and 10 inches from the nose are presented in figure 11 as a function of Mach number for the windward and leeward sides of the body.

Langley Aeronautical Laboratory,  
National Advisory Committee for Aeronautics,  
Langley Field, Va., June 14, 1957.

~~CONFIDENTIAL~~

NACA RM L57F27

## REFERENCE

1. Feller, William V.: Heat Transfer to Bodies at Angles of Attack.  
NACA RM L57D19c, 1957.

~~CONFIDENTIAL~~

TABLE I.- NOSE COORDINATES AND SKIN THICKNESS

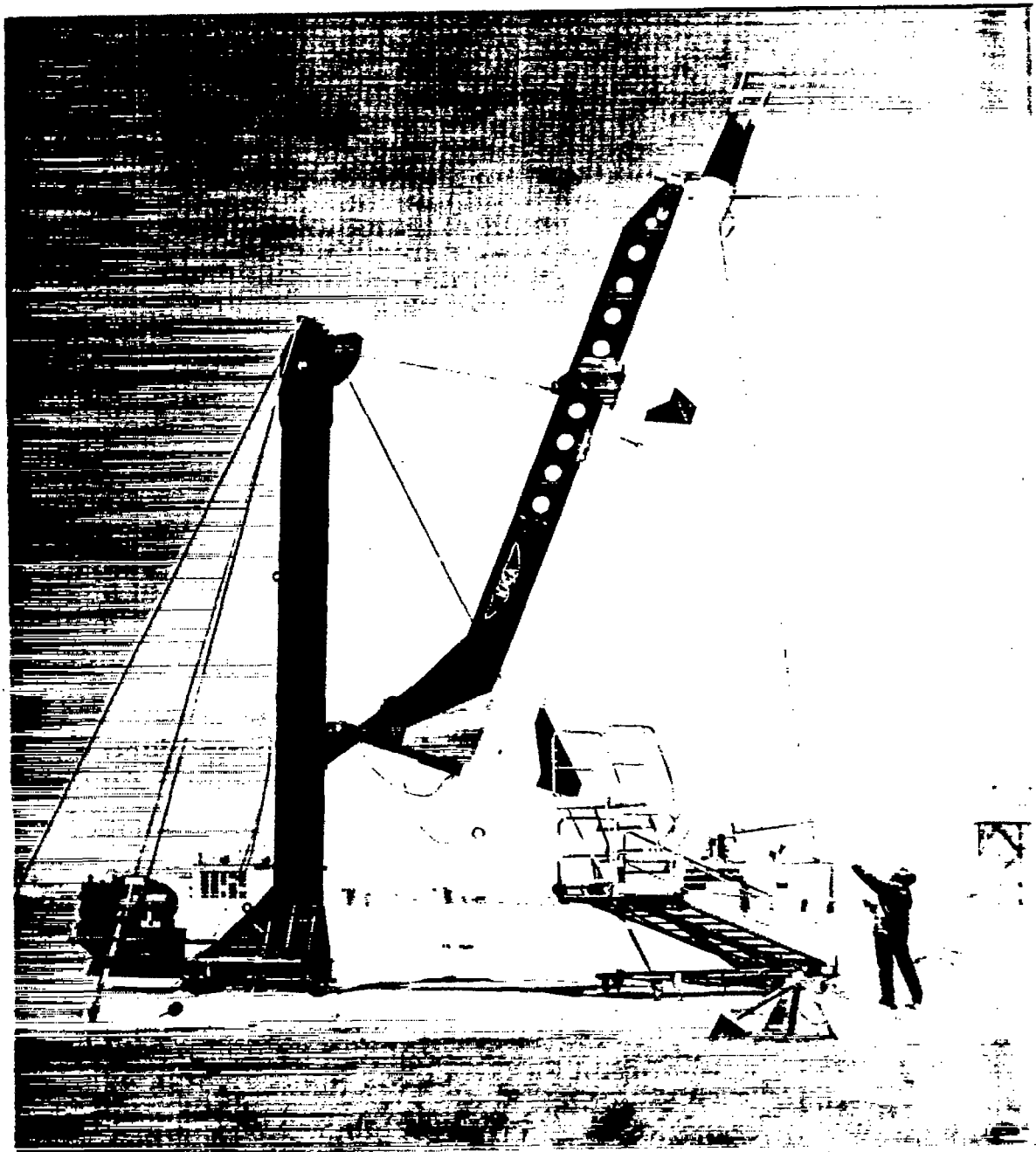
$$\Lambda = 39^\circ$$

Coordinates	
X	Y
0	0
.50	.175
1.00	.340
1.50	.497
2.00	.645
4.00	1.158
6.00	1.546
8.00	1.814
10.00	1.964
11.588	2.00
12.625	2.00

Thermocouple	Skin thickness, in.
1	0.071
2	.0295
3	.030
4	.028
5	.030
9	.032
10	.030
11	.031
15	.030
16	.030
17	.028
23	.030
24	.029
25	.030
26	.029

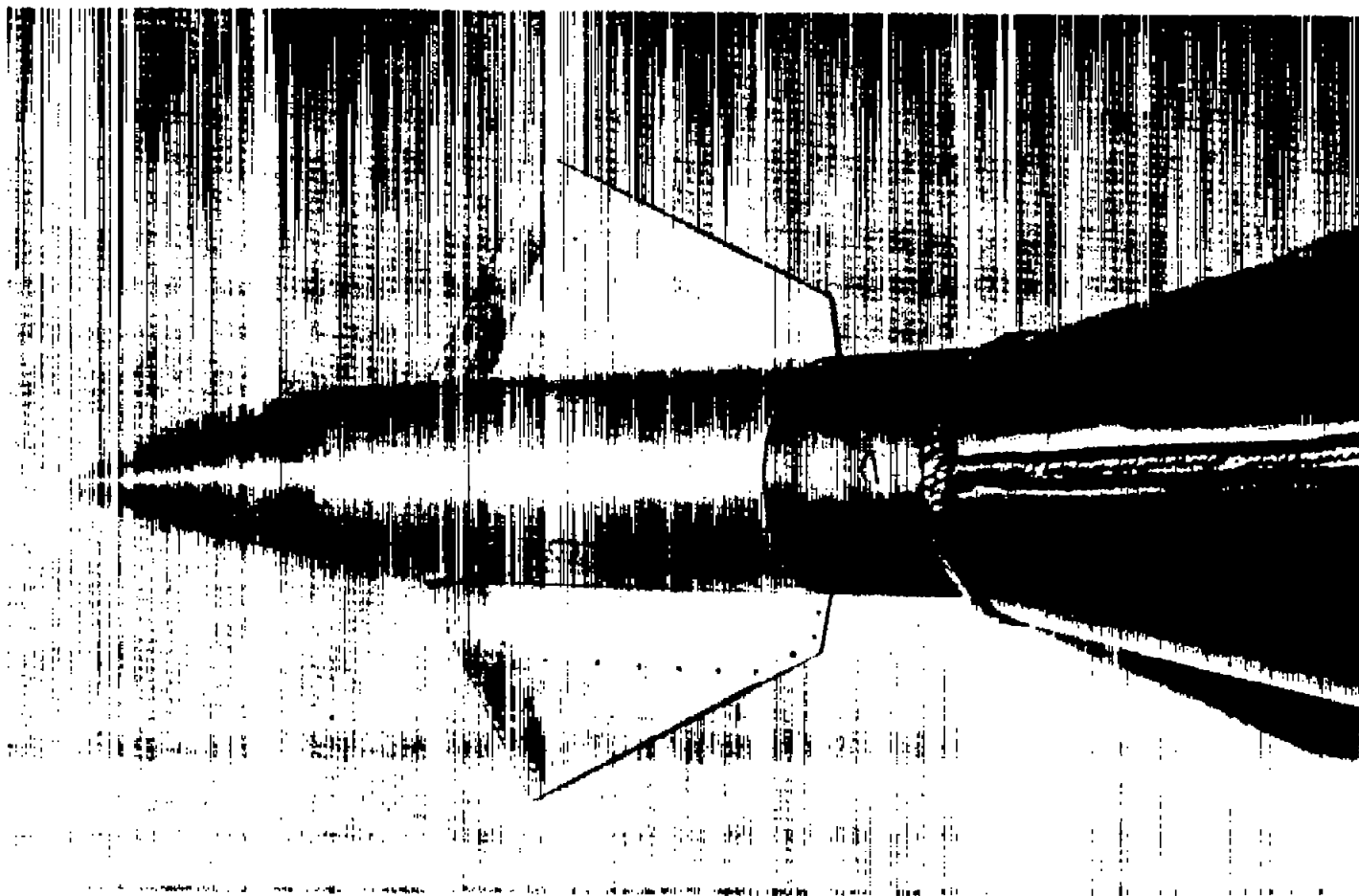
TABLE II.- THERMOCOUPLE LOCATIONS FOR WING-BODY MODELS

Thermocouple	Distance from nose tip, in.	Horizontal distance from wing leading edge, in.	$\phi$ , deg
$\Lambda = 39^\circ$			
1	0		0
2	3.0		0
3	5.0		0
4	7.5		0
5	10.0		0
6	15.37		0
7	19.37		0
8	23.57		0
9	5.0		270.0
10	10.0		270.0
11	5.0		315.0
12	15.37	1	270.0
13	19.37	5.1	270.0
14	23.57	9.3	270.0
15	10.0		315.0
16	5.0		225.0
17	10.0		225.0
18	15.37		67.5
19	19.37		67.5
20	23.57		67.5
21		0	
22	19.37		45.0
23	3.0		180.0
24	5.0		180.0
25	7.5		180.0
26	10.0		180.0
27	15.37		180.0
28	19.37		180.0
29	23.57		180.0
30	15.37		247.5
31	19.37		247.5
32	23.57		247.5
33	15.37	1	90.0
34	19.37	5.1	90.0
35	23.57	9.3	90.0
$\Lambda = 75^\circ$			
36	15.87		292.5
37	20.47		292.5
38	23.57		292.5
39	15.87	1.1	270.0
40	20.47	5.7	270.0
41	23.57	8.8	270.0
42		0	
43	15.87		180.0
44	20.47		180.0
45	23.57		180.0
46	15.87		112.5
47	20.47		112.5
48	23.57		112.5
49		1.1	90.0
50		5.7	90.0
51		8.8	90.0



(a) Configuration in launching position. L-57-1394

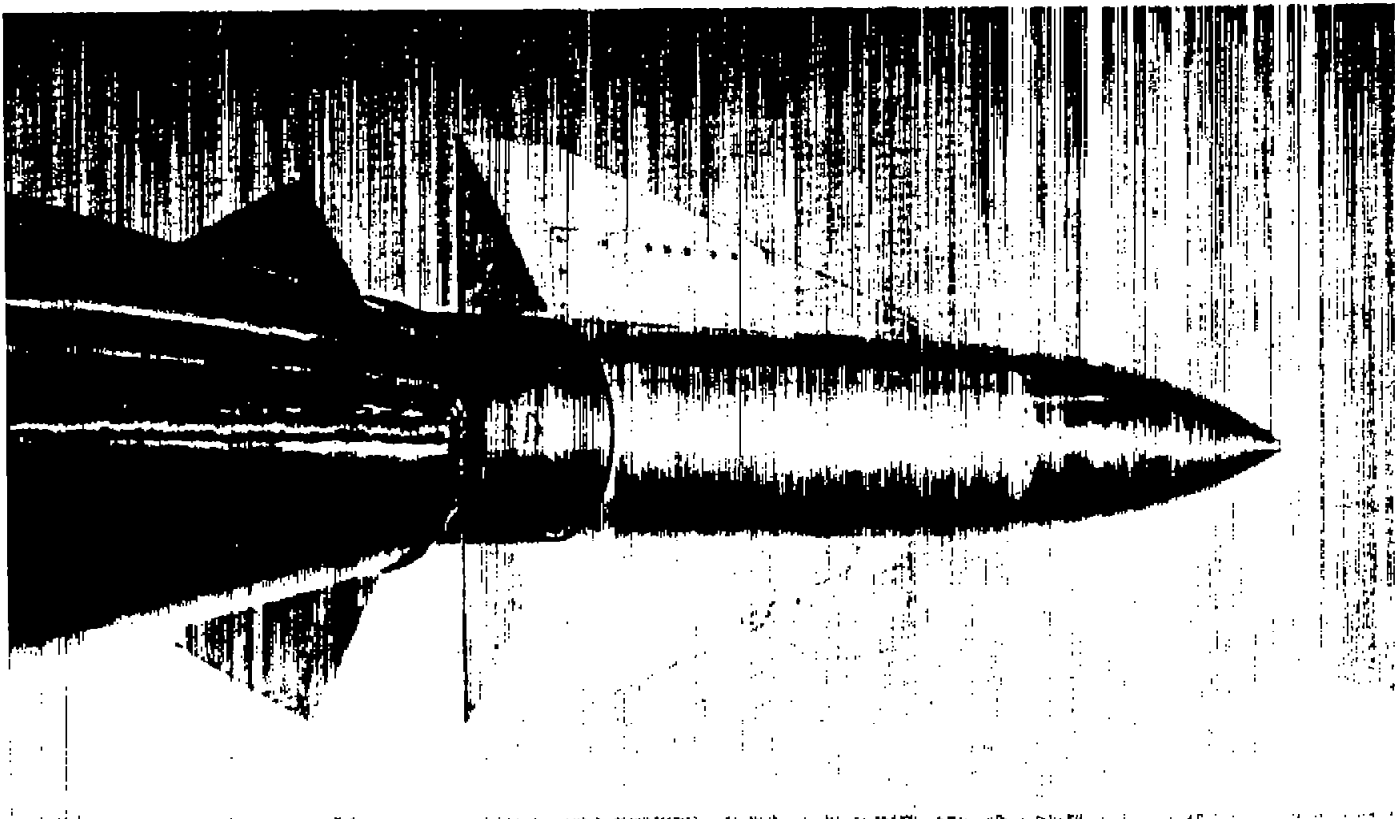
Figure 1.- Photographs of models.



(b) Model with  $39^\circ$  swept wing.

L-96373

Figure 1.- Continued.

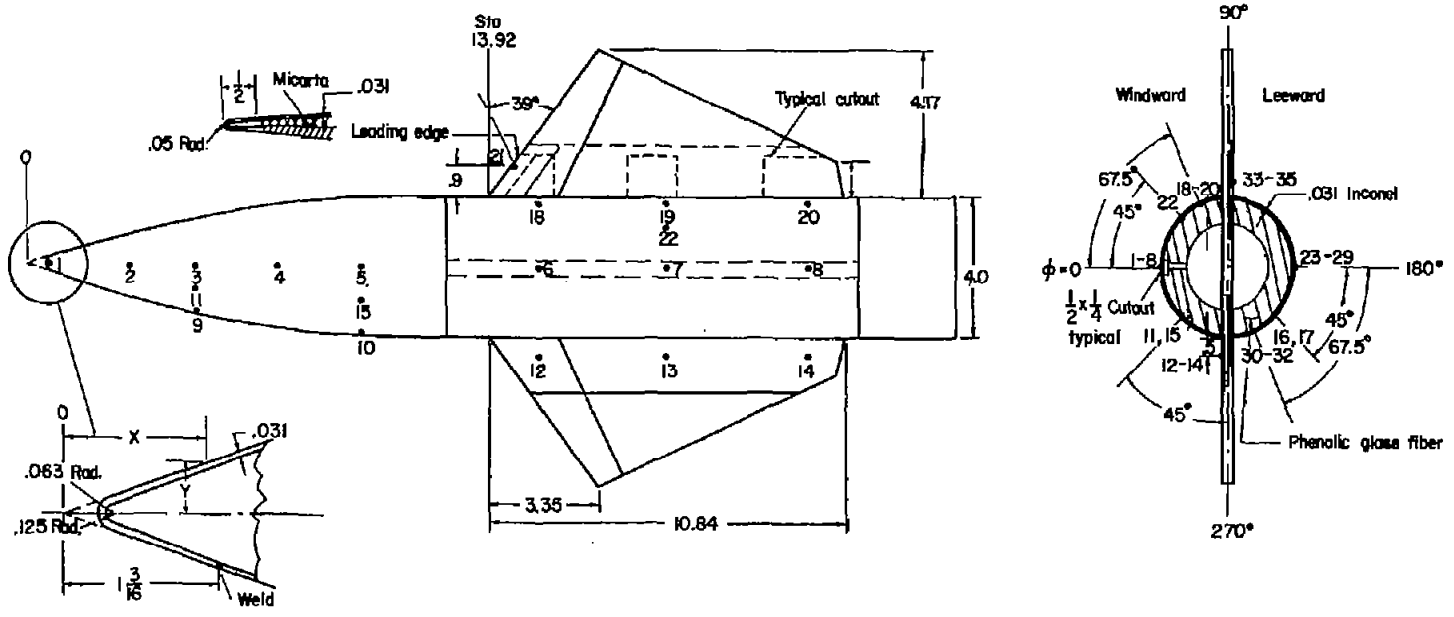


(c) Model with 75° swept wing.

L-96372

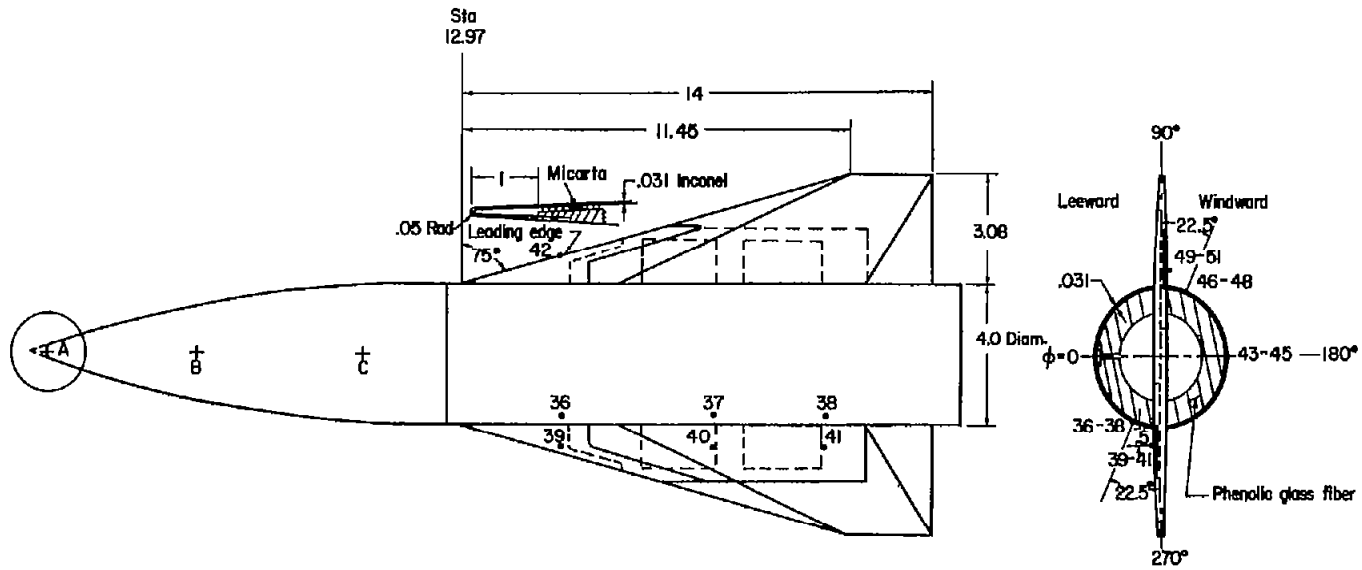
Figure 1.- Concluded.

CONFIDENTIAL



(a)  $\Lambda = 39^\circ$ .

Figure 2.- Sketch of models with thermocouple locations shown. (All dimensions are in inches unless otherwise noted.)



All wing temperature panels insulated from wing structure by  $\frac{1}{32}$  Micarta.

(b)  $\Lambda = 75^\circ$ .

Figure 2.- Concluded.

CONFIDENTIAL

CONFIDENTIAL

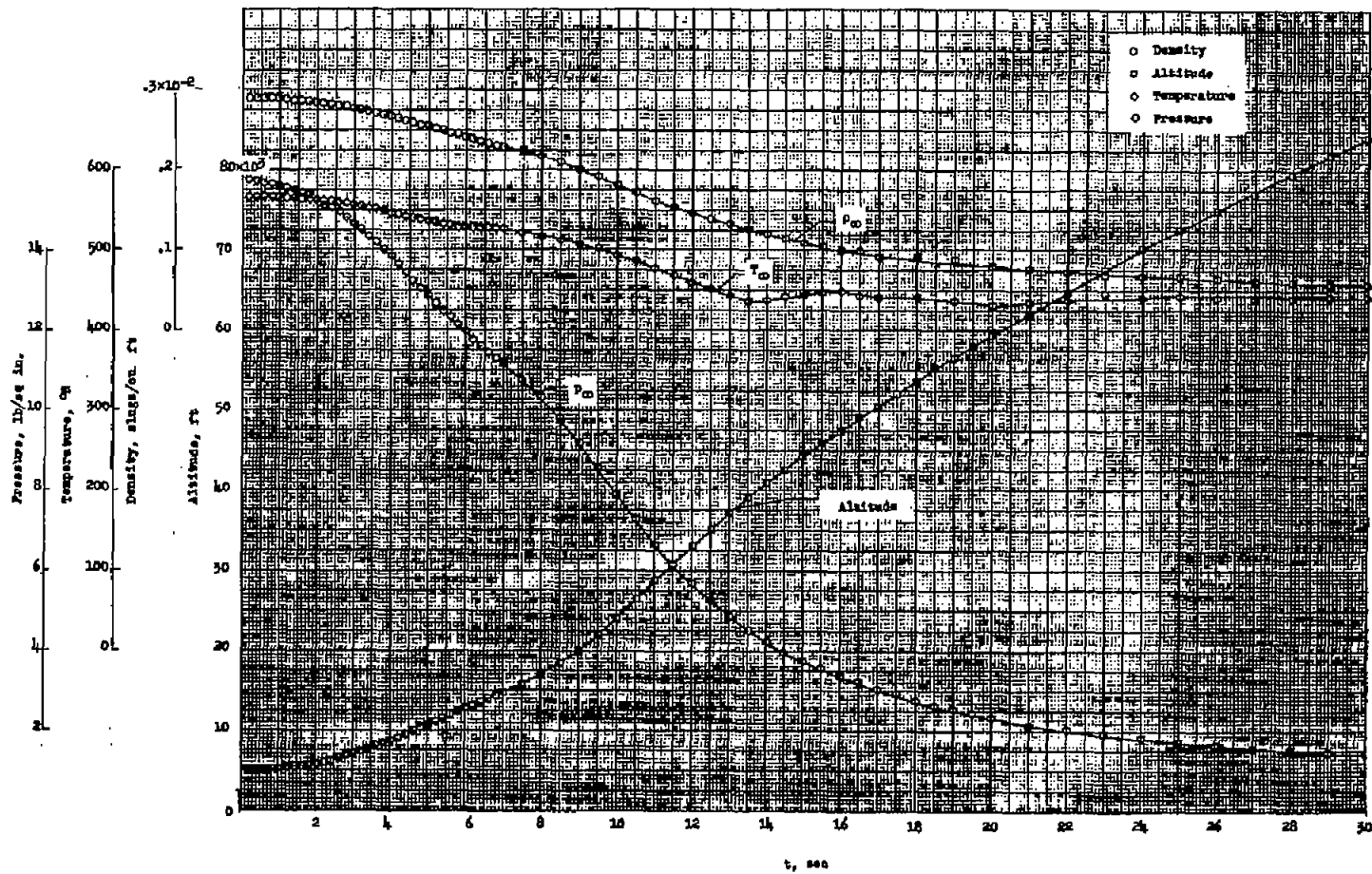


Figure 3.- Atmospheric conditions and altitude time histories.

~~CONFIDENTIAL~~

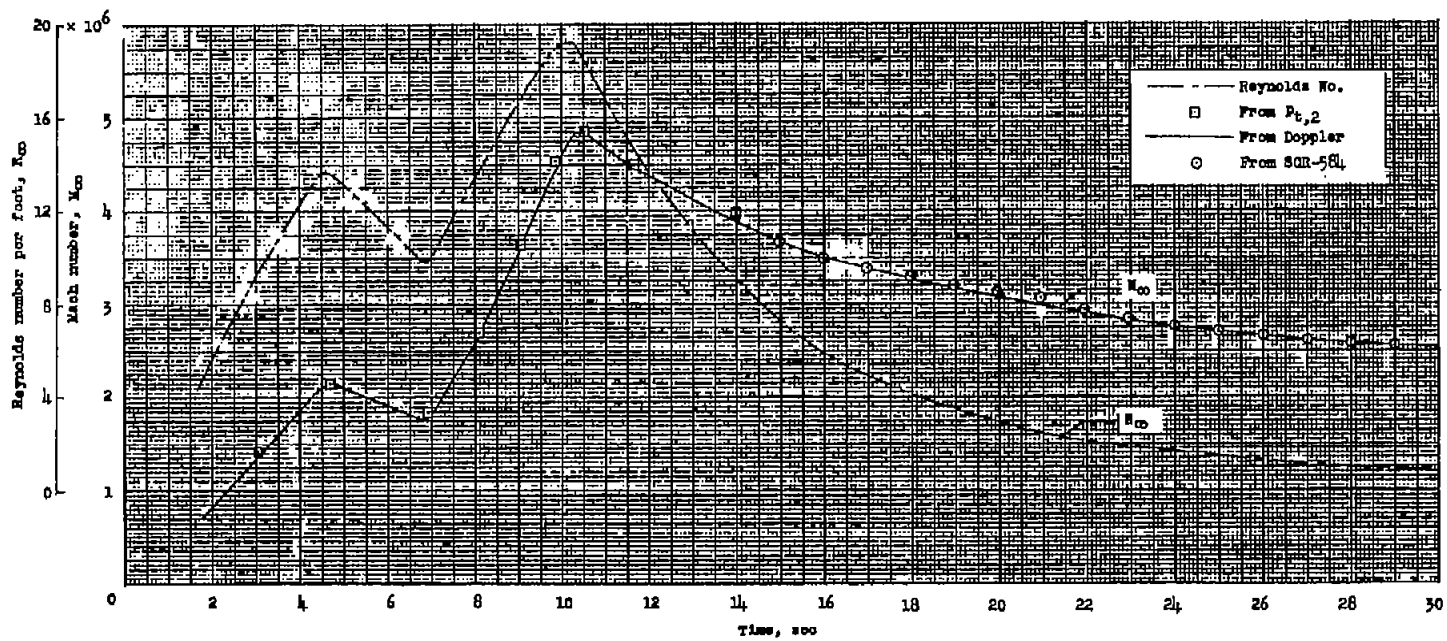
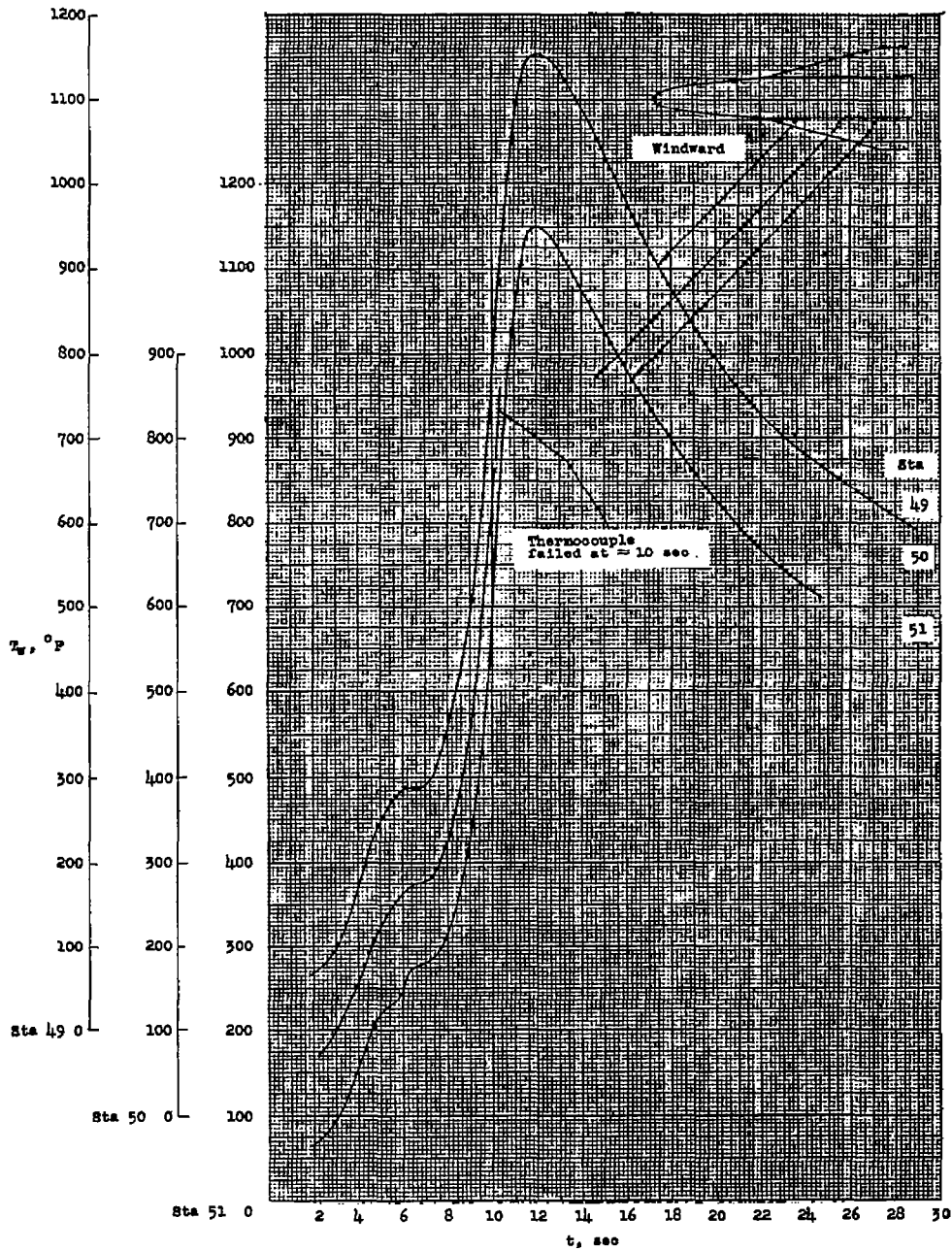


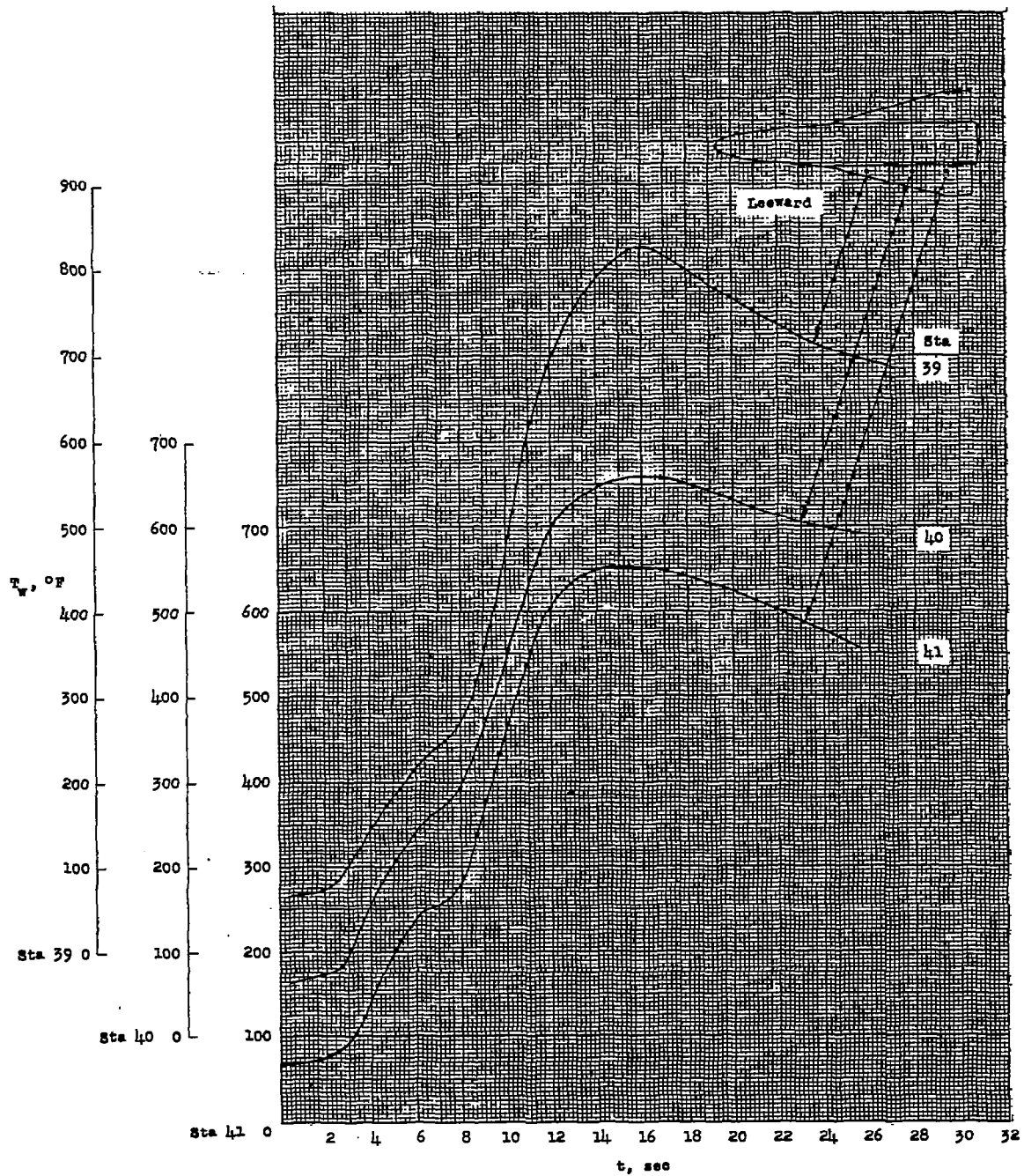
Figure 4.- Mach number and free-stream Reynolds number per foot.

CONFIDENTIAL



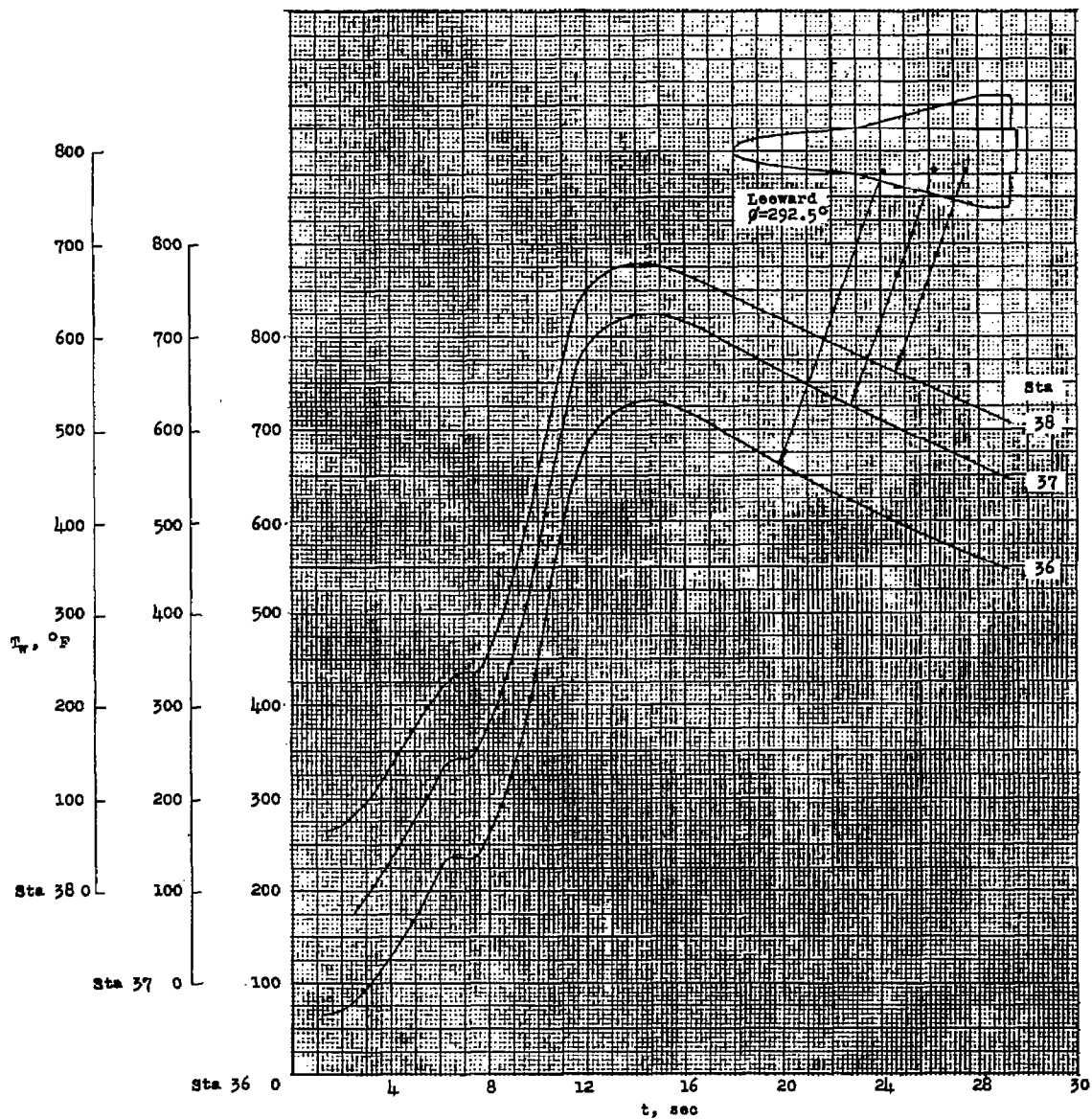
(a) Stations 49, 50, and 51.

Figure 5.- Temperature time histories for the  $75^{\circ}$  swept-wing model.



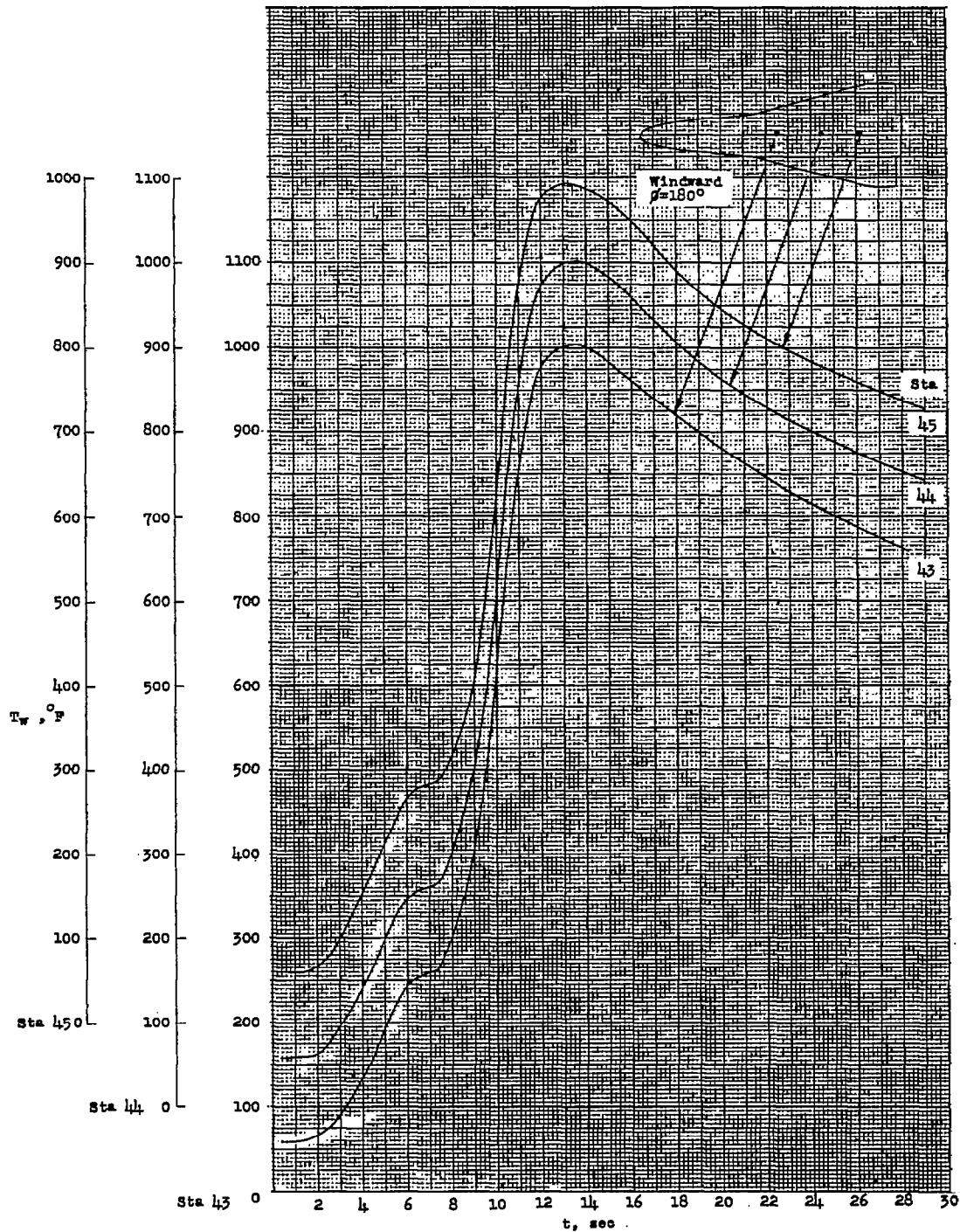
(b) Stations 39, 40, and 41.

Figure 5.- Continued.



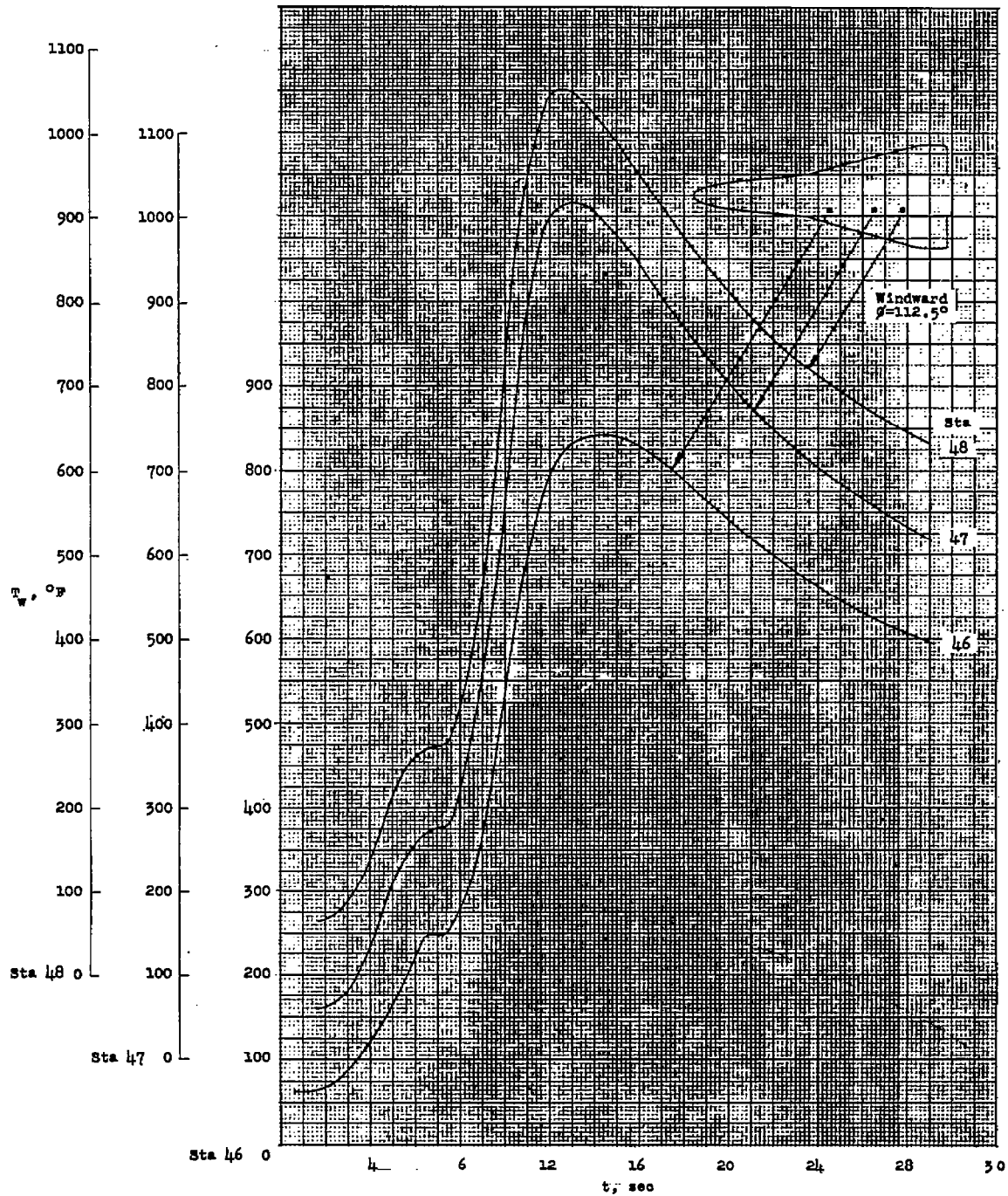
(c) Stations 36, 37, and 38.

Figure 5.- Continued.



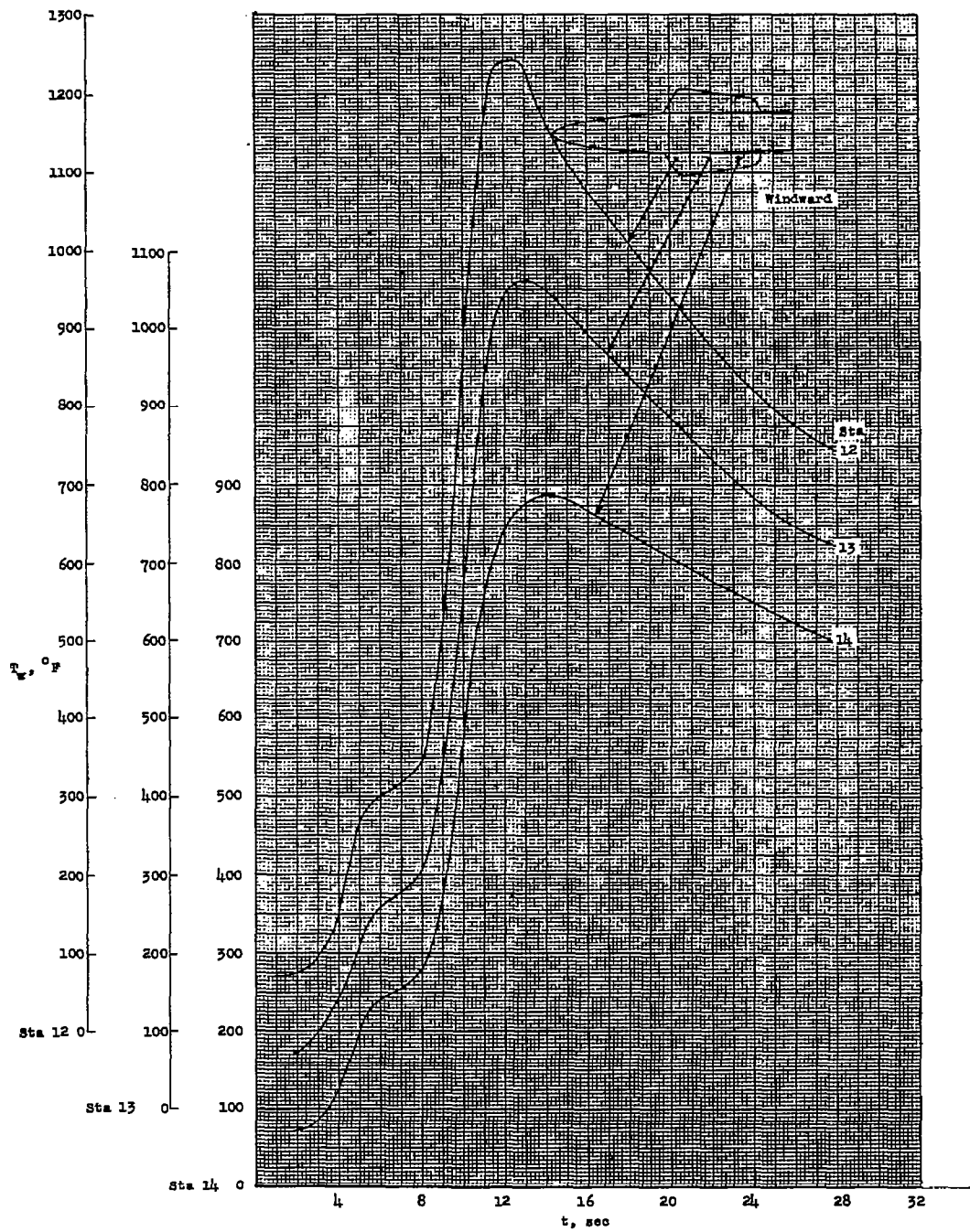
(d) Stations 43, 44, and 45.

Figure 5.- Continued.



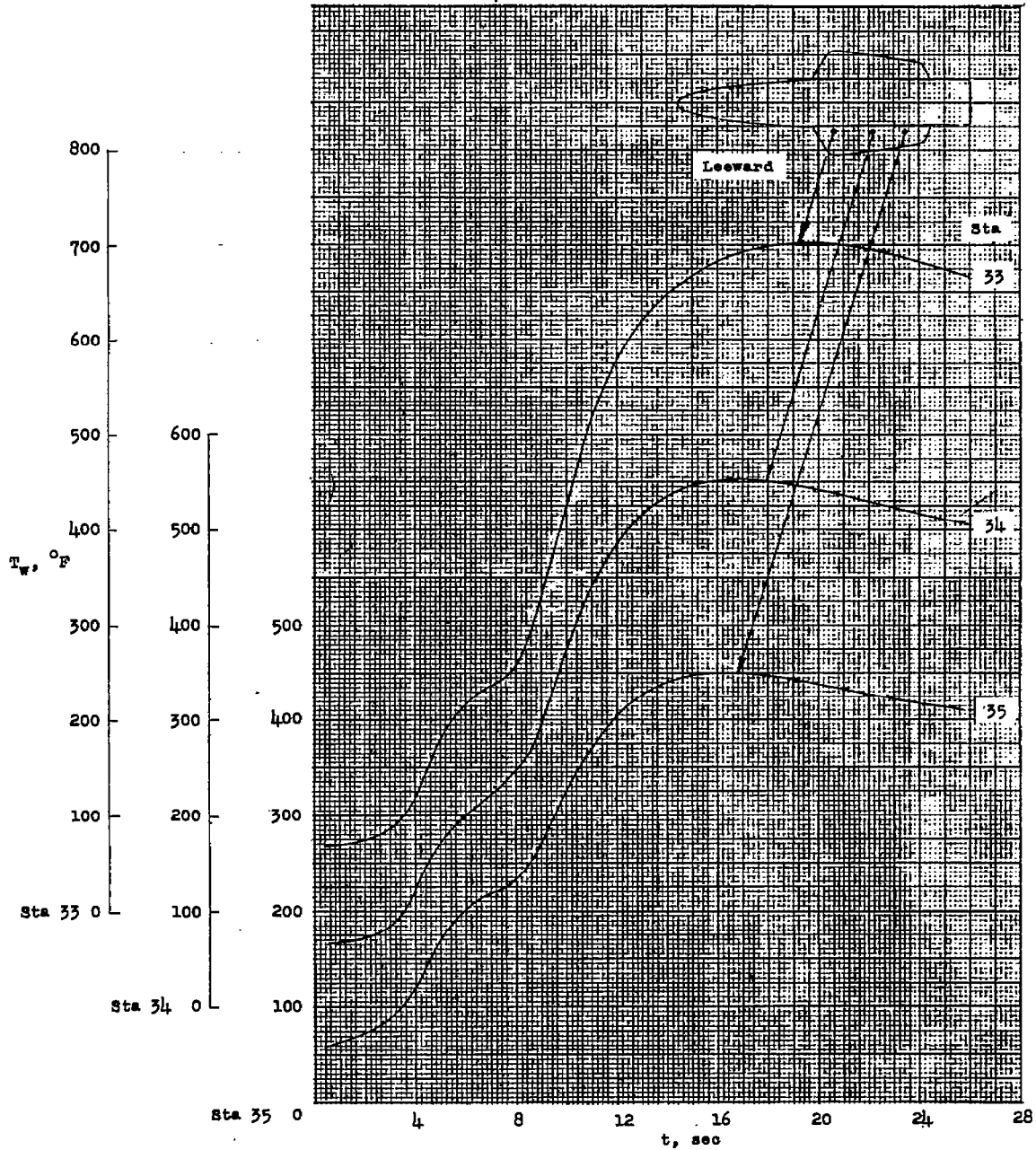
(e) Stations 46, 47, and 48.

Figure 5.- Concluded.



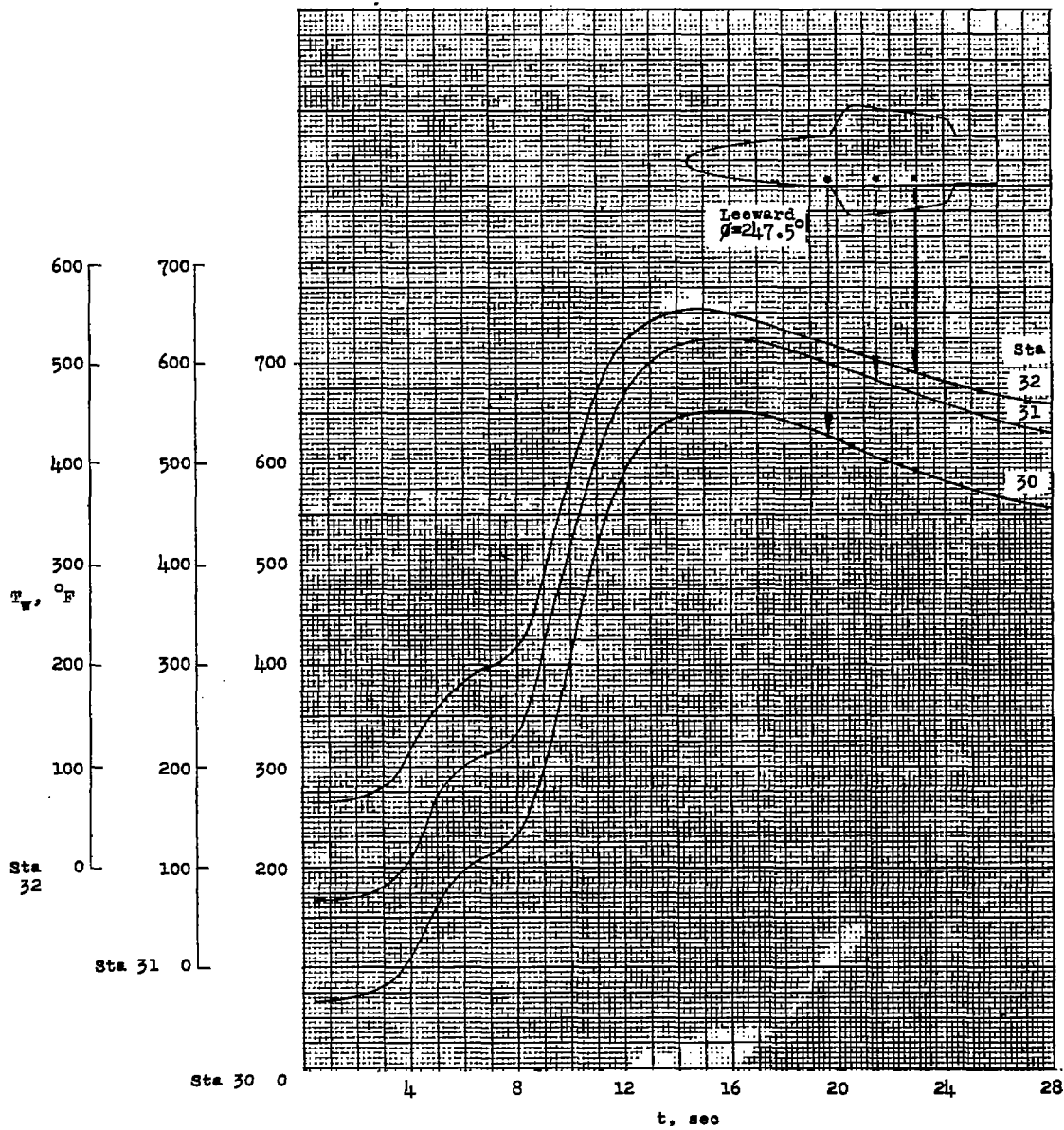
(a) Stations 12, 13, and 14.

Figure 6.- Temperature time histories for the 39° swept-wing model.



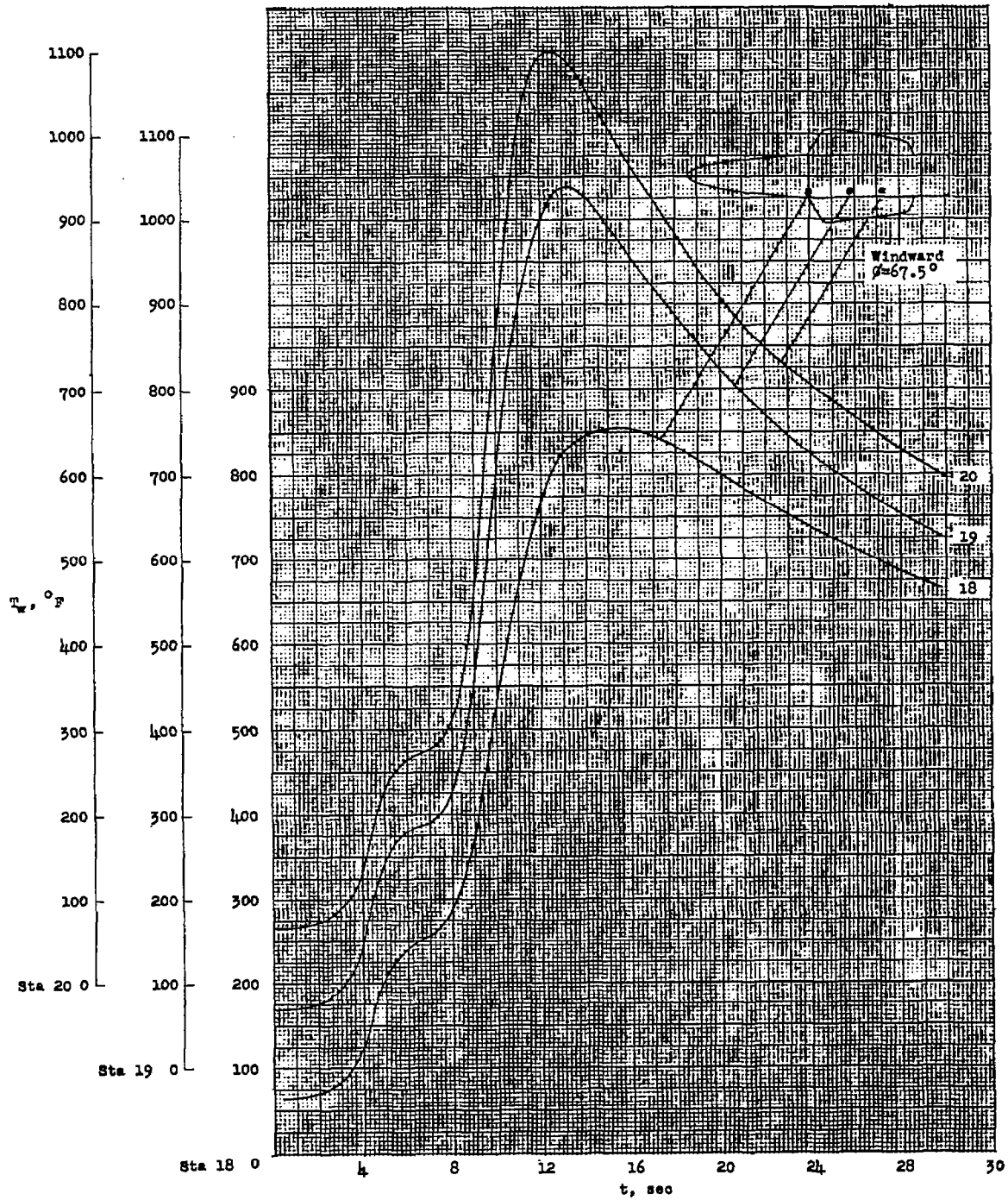
(b) Stations 33, 34, and 35.

Figure 6.- Continued.



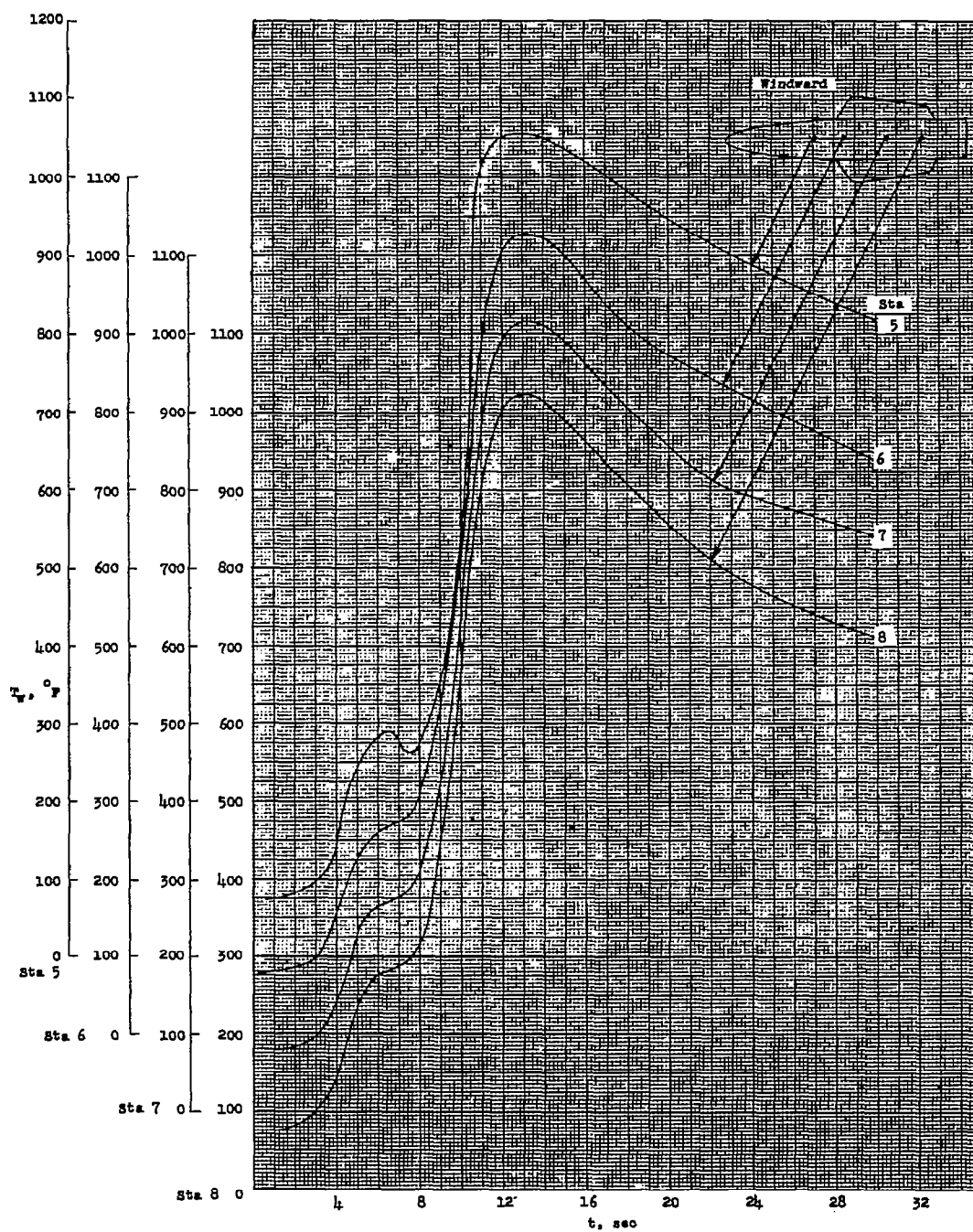
(c) Stations 30, 31, and 32.

Figure 6.- Continued.



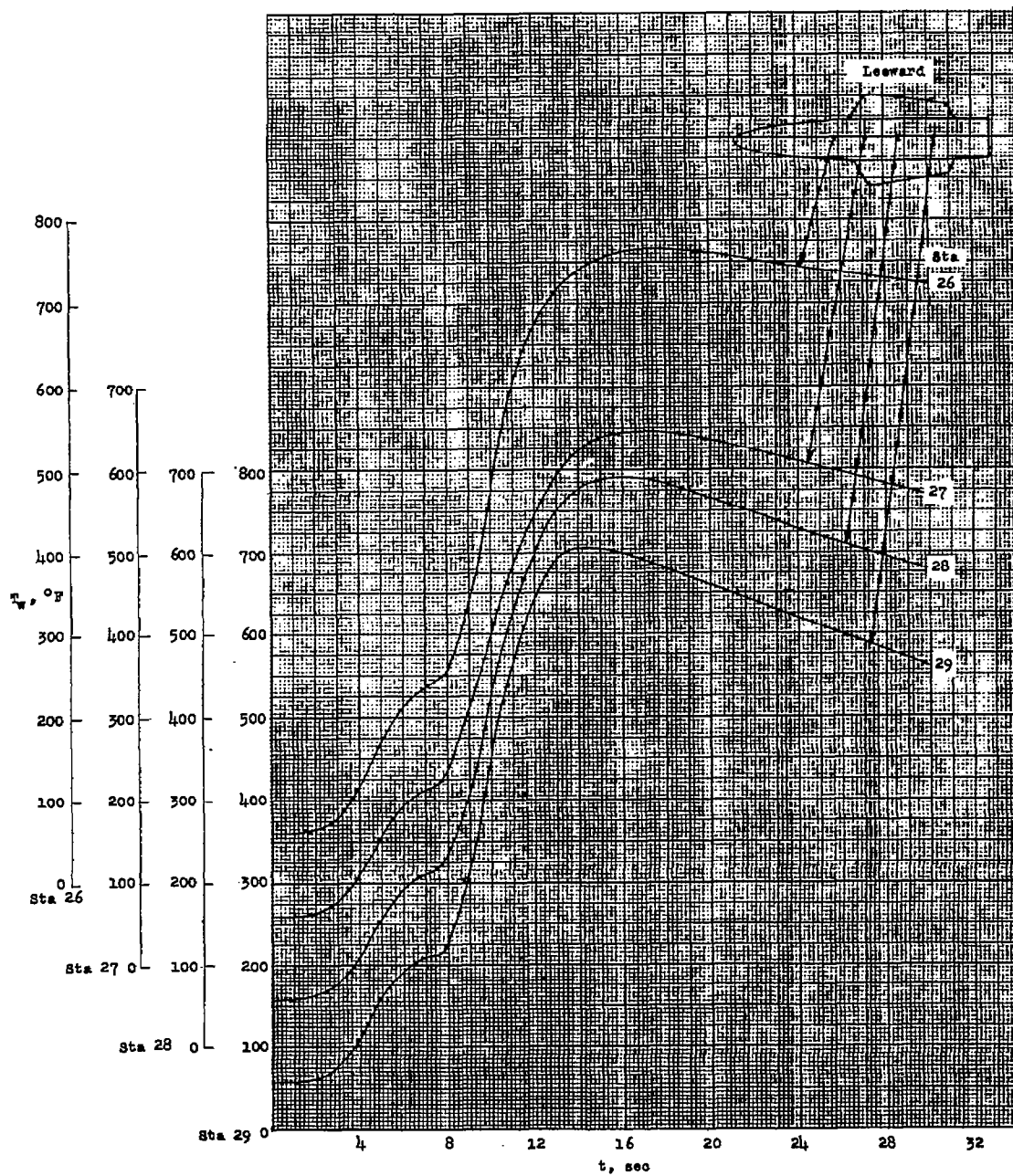
(d) Stations 18, 19, and 20.

Figure 6.- Continued.



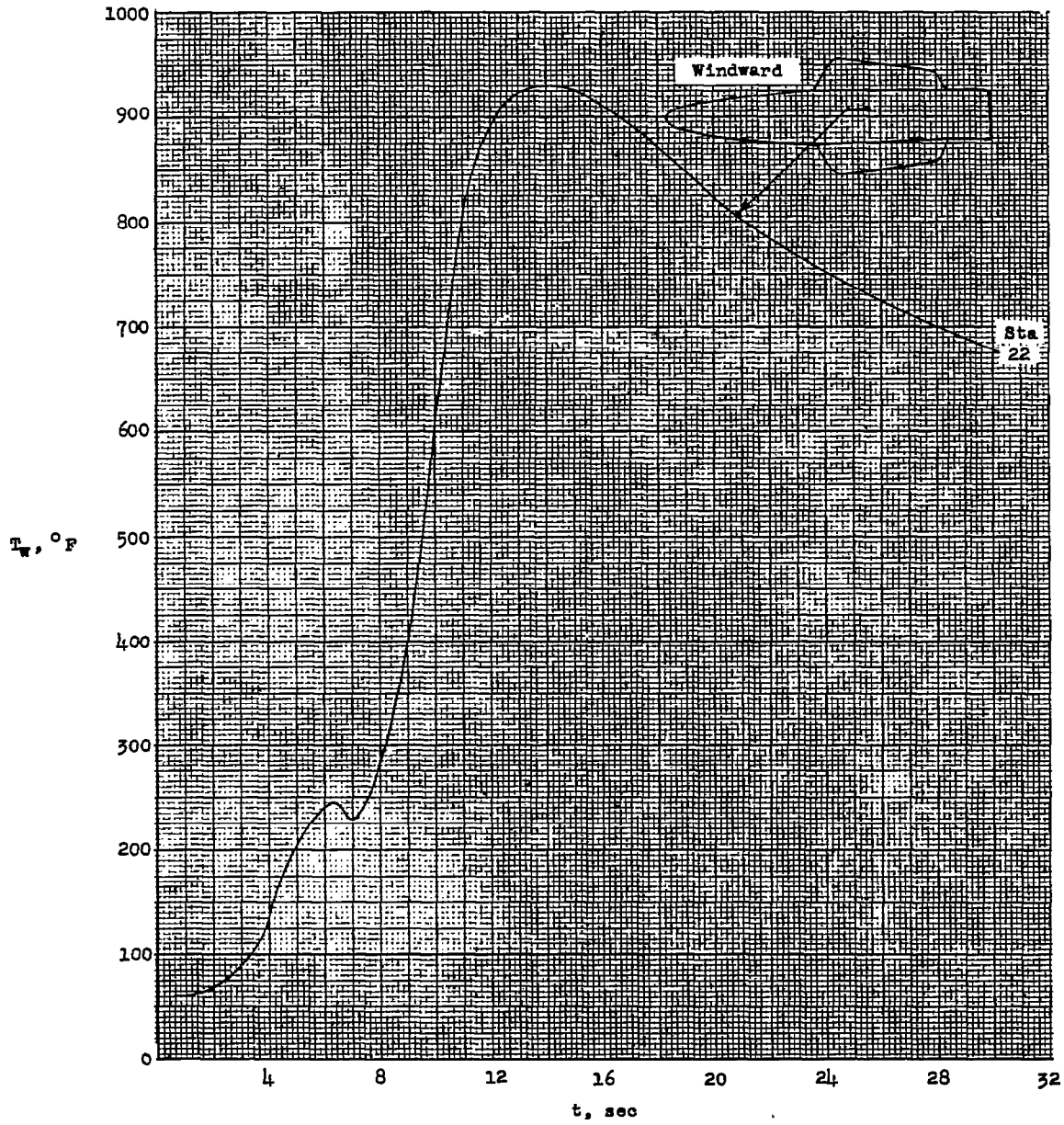
(e) Stations 5, 6, 7, and 8.

Figure 6.- Continued.



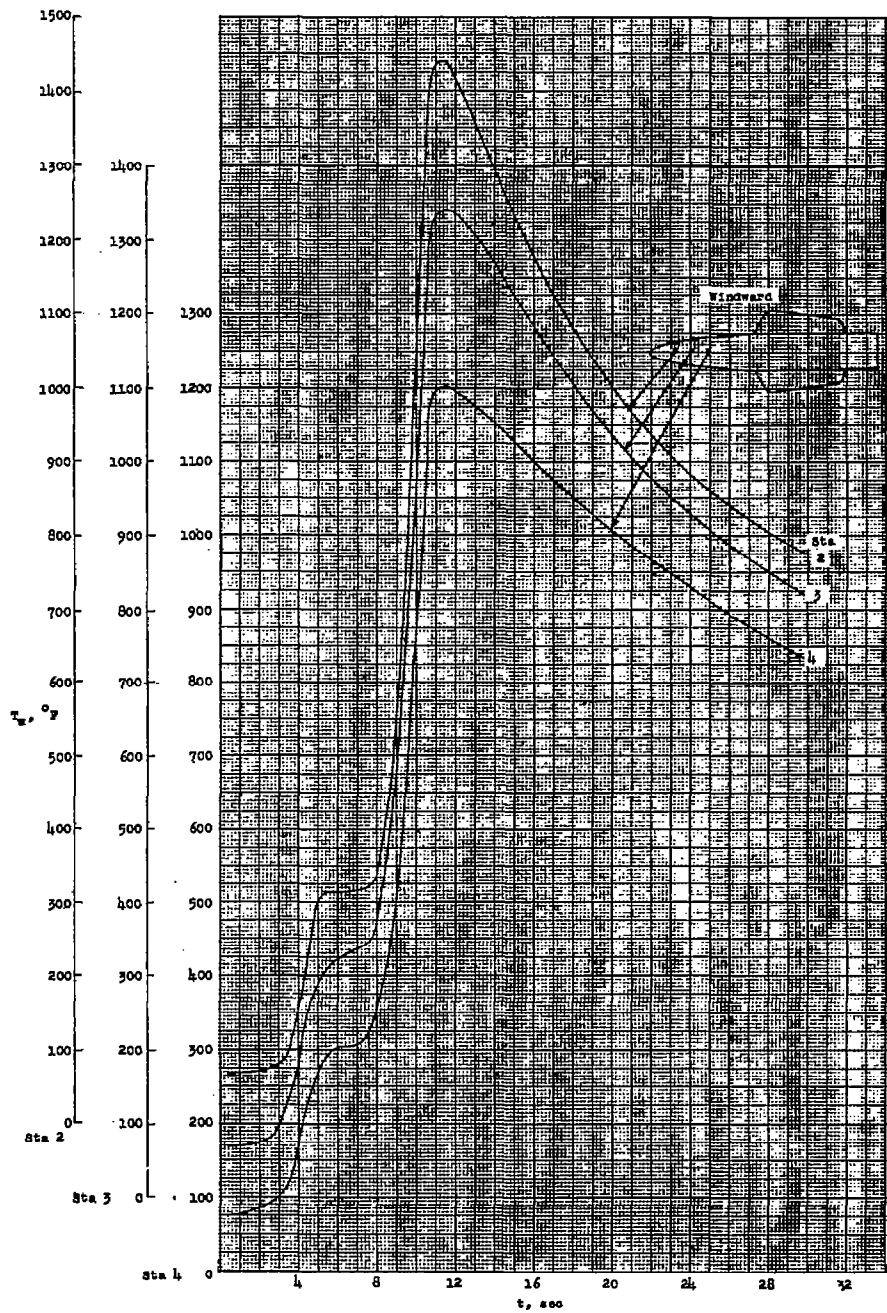
(f) Stations 26, 27, 28, and 29.

Figure 6.- Continued.



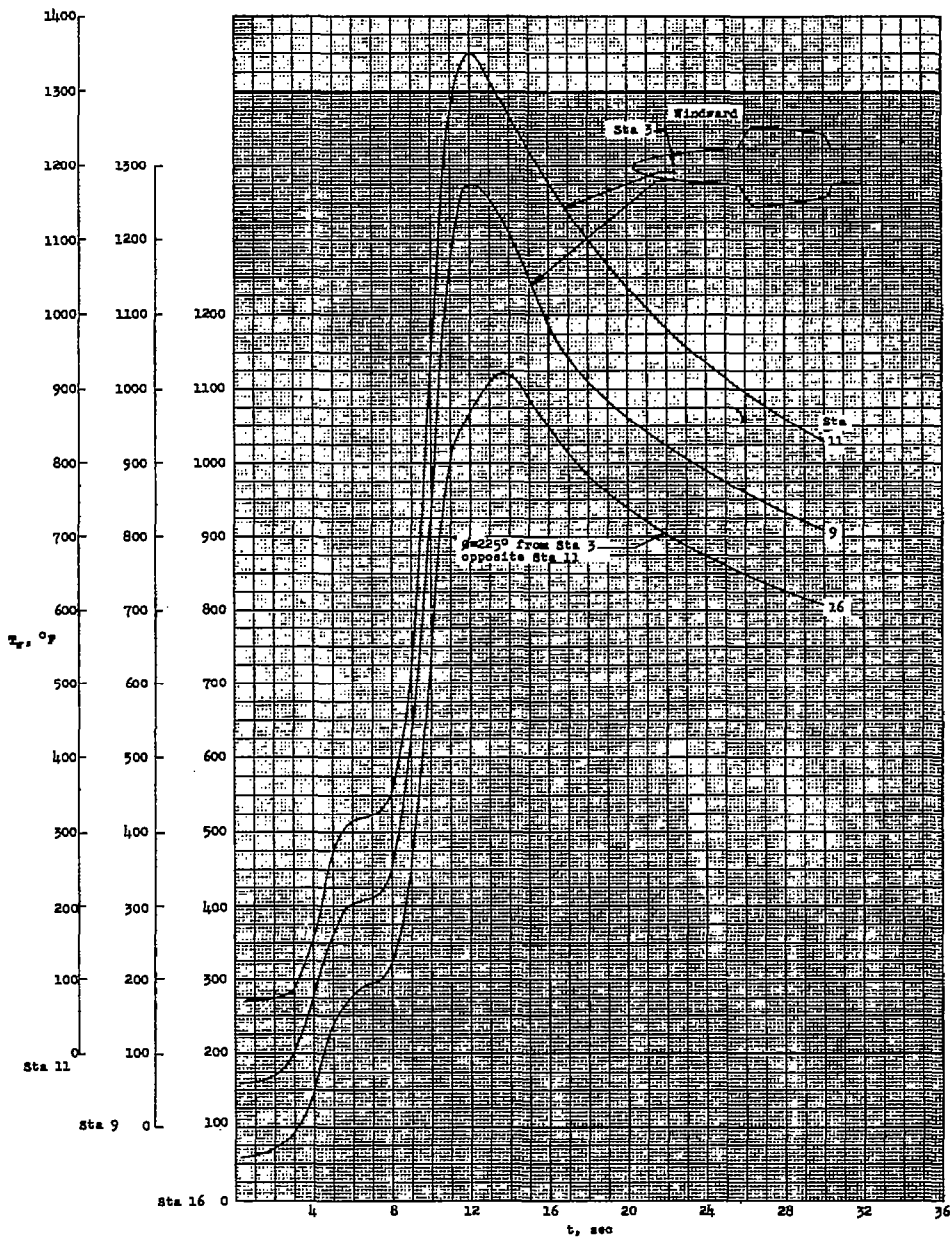
(g) Station 22.

Figure 6.- Continued.



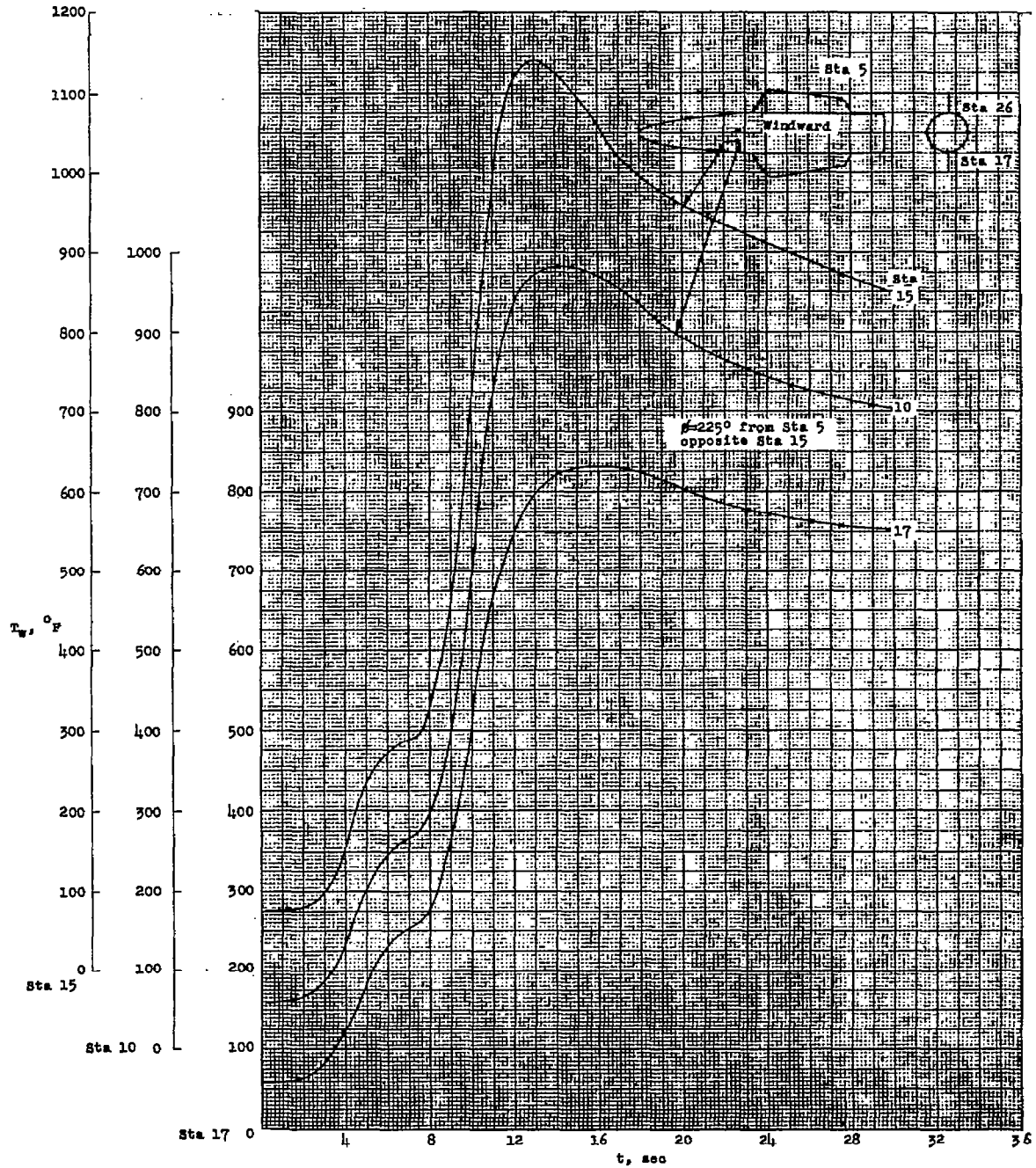
(h) Stations 2, 3, and 4.

Figure 6.- Continued.



(i) Stations 9, 11, and 16.

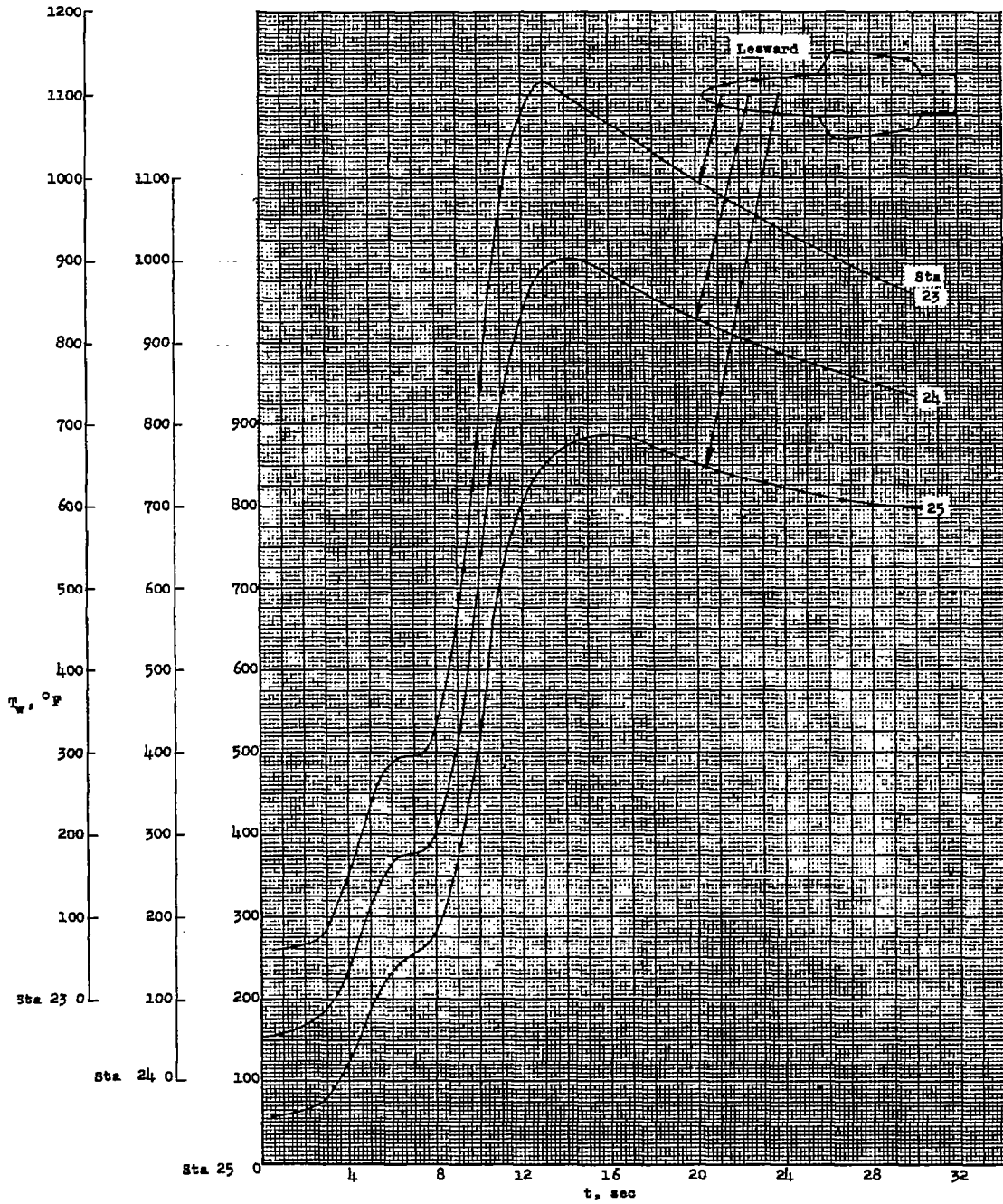
Figure 6.- Continued.



(j) Stations 10, 15, and 17.

Figure 6.- Continued.

~~CONFIDENTIAL~~  
CONFIDENTIAL



(k) Stations 23, 24, and 25.

Figure 6.- Concluded.

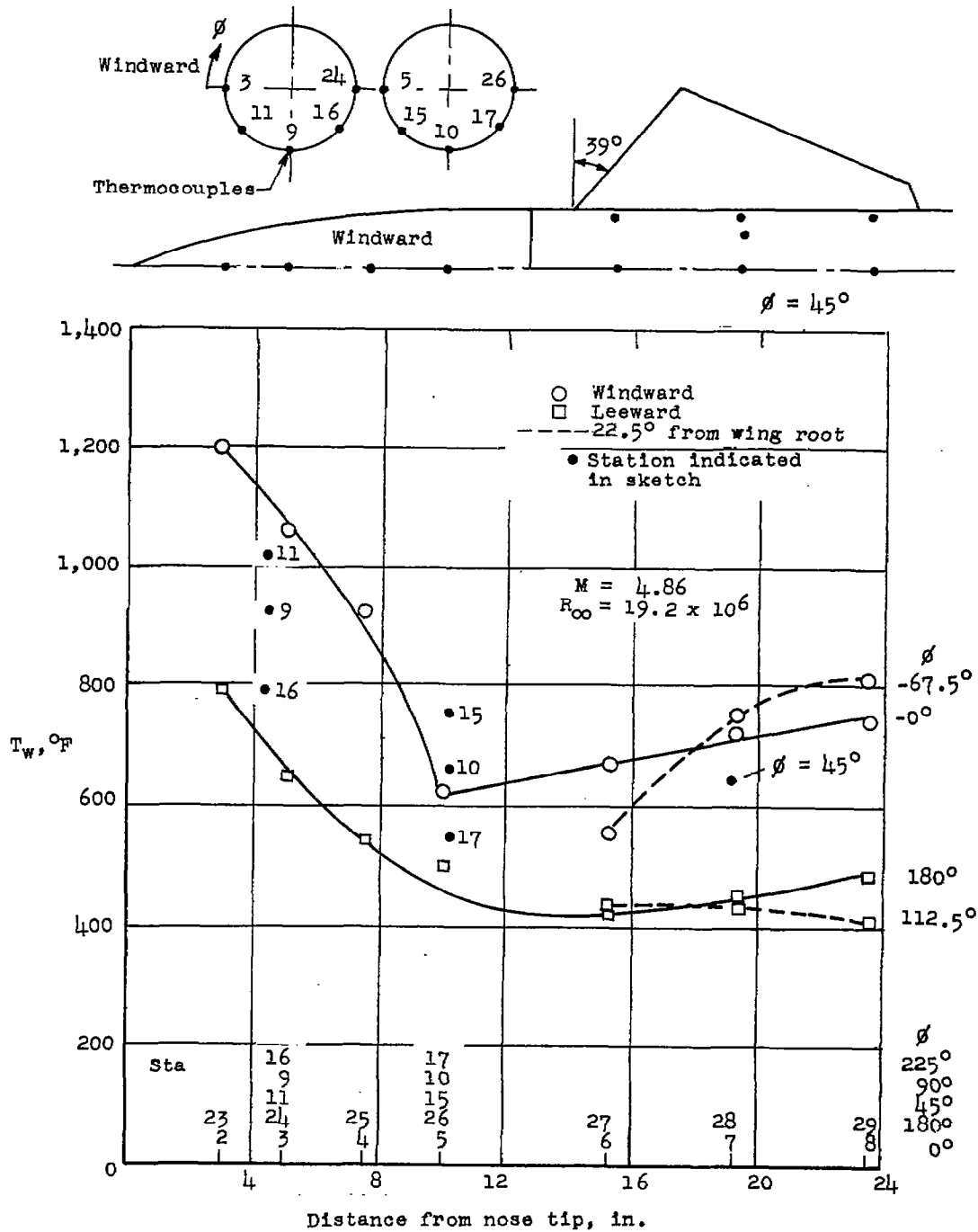


Figure 7.- Temperature distribution along the body and at wing-body juncture for wing-body model with  $\Delta = 39^\circ$ .  $\alpha = 7^\circ$ .

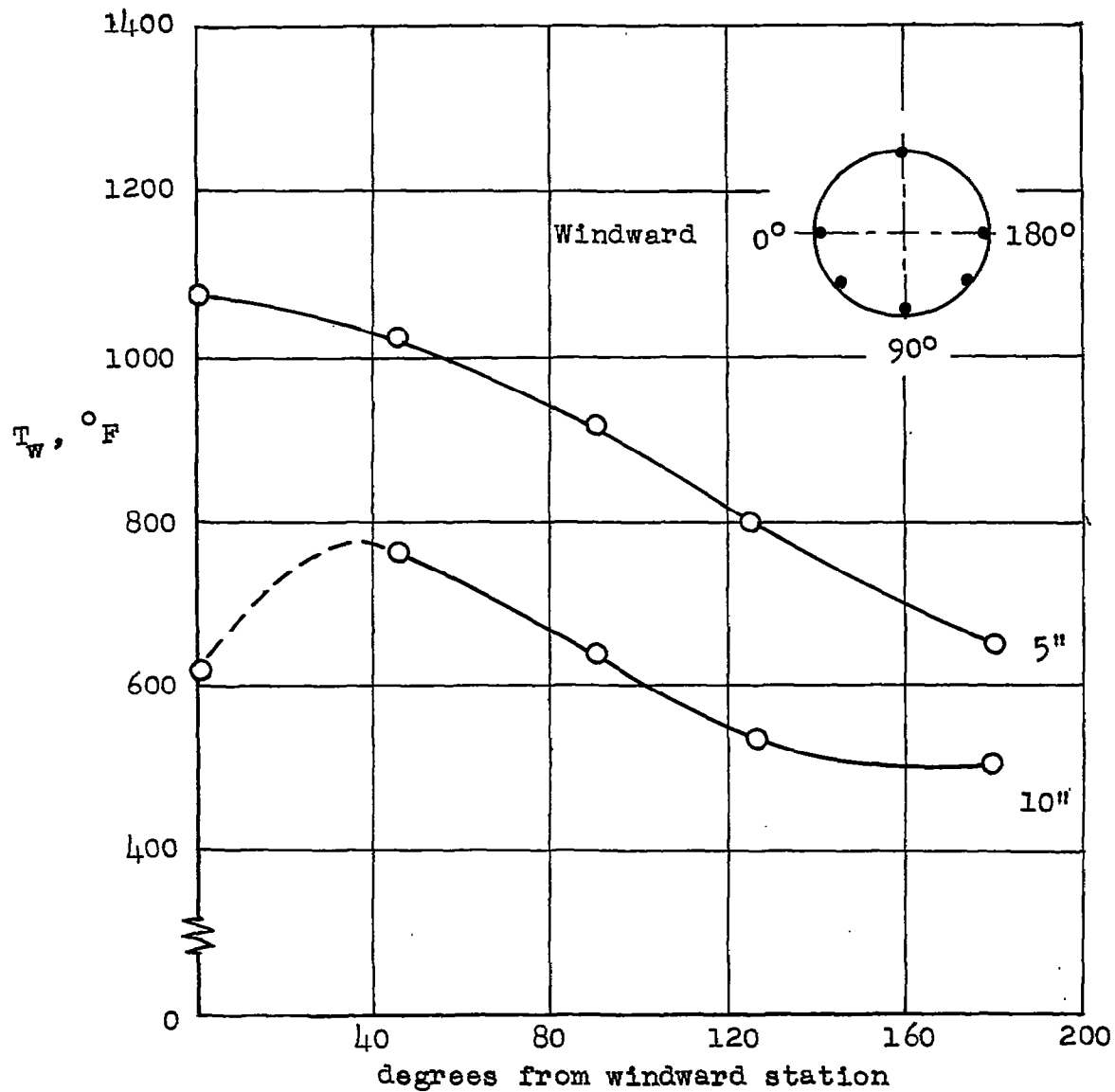


Figure 8.- Distribution of temperature around body at 5 and 10 inches from the nose.  $M = 4.86$ .

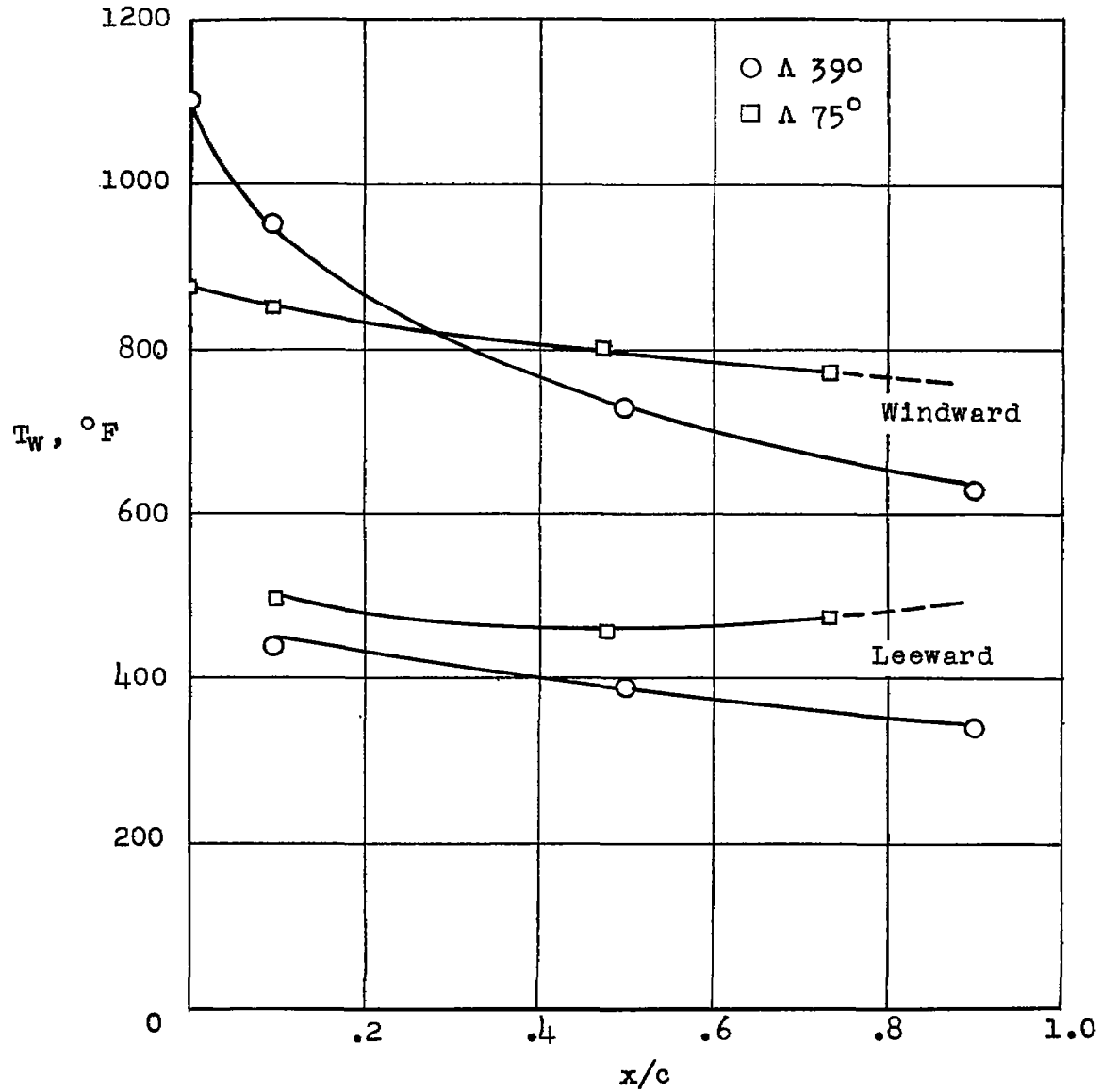


Figure 9.- Temperature distribution on the upper and lower surfaces of wings at  $\alpha = 7^\circ$ .  $M = 4.86$ .

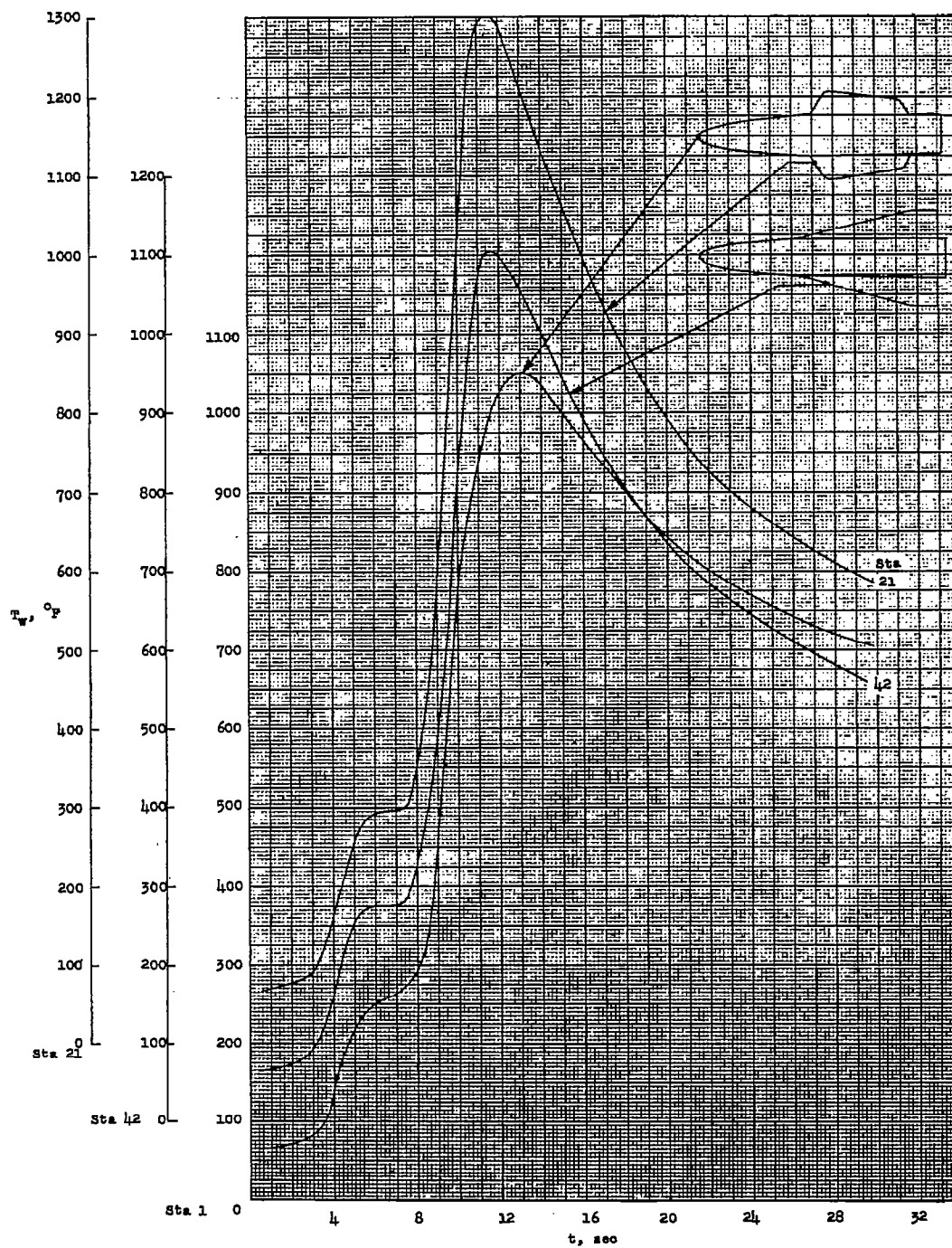


Figure 10.- Time histories of leading-edge temperature for the  $39^\circ$  and  $75^\circ$  swept wing and for the body stagnation point.

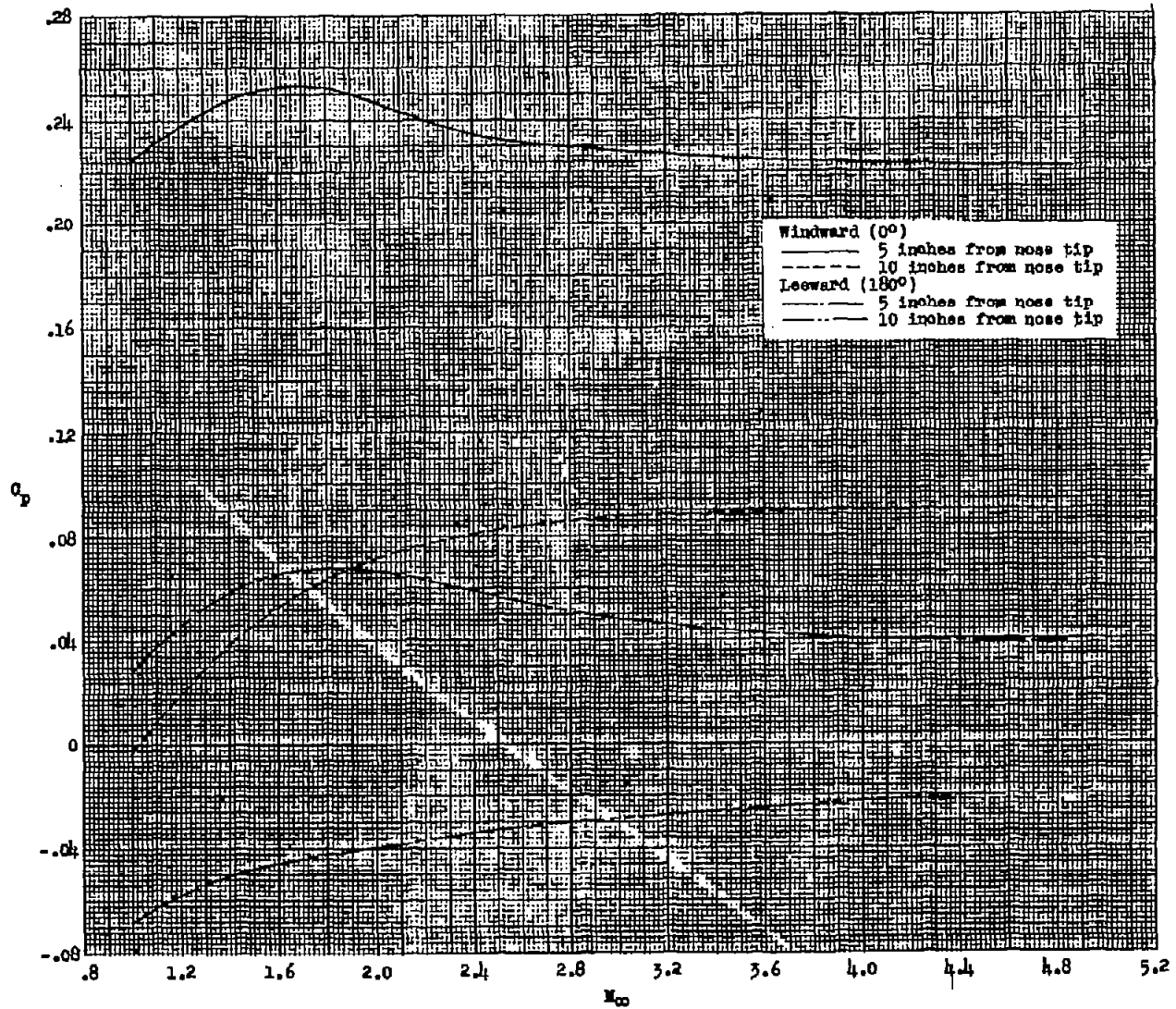


Figure 11.- Pressure coefficients for stations at 5 and 10 inches from nose.